Historical and Projected Eastern Pacific and Intra-Americas Sea TD-Wave Activity in a Selection of IPCC AR5 Models

YOLANDE L. SERRA

Joint Institute for the Study of the Atmosphere and Ocean, University of Washington, Seattle, Washington

KERRIE GEIL

Department of Hydrology and Atmospheric Sciences, The University of Arizona, Tucson, Arizona

(Manuscript received 15 June 2016, in final form 3 October 2016)

ABSTRACT

The tracks of westward-propagating synoptic disturbances across the Intra-Americas Sea (IAS) and far-eastern Pacific, known as easterly waves or tropical depression (TD) waves, are an important feature of the region's climate. They are associated with heavy rainfall events, seed the majority of tropical cyclones, and contribute to the mean rainfall across the region. This study examines the ability of current climate models (CMIP5) to simulate TD-wave activity and associated environmental factors across the IAS and far-eastern Pacific as compared to reanalysis. Model projections for the future are then compared with the historical model experiment to investigate the southward shift in CMIP5 track density and the environmental factors that may contribute to it. While historical biases in TD-wave track-density patterns are well correlated with model biases in sea surface temperature and midlevel moisture, the projected southward shift of the TD track density by the end of the twenty-first century in CMIP5 models is best correlated with changes in deep wind shear and midlevel moisture. In addition, the genesis potential index is found to be a good indicator of both present and future regions of high TD-wave track density for the models in this region. This last result may be useful for understanding the more complex relationship between tropical cyclones and this index in models found in other studies.

1. Introduction

During boreal summer, easterly waves (Riehl 1945) are an important climatic feature of the Intra-Americas Sea (IAS) region and tropical far-eastern North Pacific. These disturbances bring heavy rainfall to Central America, southern Mexico, and the Caribbean region (Amador et al. 2006) and seed the majority of tropical cyclones (TCs) in the tropical Atlantic and eastern Pacific (Landsea 1993; Avila and Pasch 1995). TD waves have also been suggested to be the "building blocks" of the climatological ITCZ (Holton et al. 1971; Toma and Webster 2010) and are considered important to the mean precipitation patterns of the IAS. Takayabu and Nitta (1993) and Dunkerton and Baldwin (1995) referred to such systems as "TD type" waves for their relationship to tropical depressions (TDs), and both the easterly wave (EW) and TD-wave terminology are used interchangeably here.

Current understanding of TD waves suggests that they share similarities with the moisture mode instability that develops in very simplified models of tropical convection and its interaction with the large-scale flow (Sobel et al. 2001; Raymond and Fuchs 2007; Raymond et al. 2015). In these models convective heating is balanced by vertical motion, and moisture effects on the moist static energy perturbations are of primary importance for the growth and maintenance of these convectively coupled instabilities (Kuang 2011; Yasunaga and Mapes 2012; Raymond et al. 2015). Gridded observations of TD waves in the eastern Pacific suggest that the conversion of eddy available potential energy (from latent heating coupled to the waves) to eddy kinetic energy is an important process maintaining the waves as they propagate across this region (Maloney and Hartmann 2001; Maloney and Dickinson 2003; Serra et al. 2008, 2010; Crosbie and Serra 2014; Rydbeck and Maloney 2014), consistent with the conceptual model of these waves that is emerging in the literature. Barotropic instabilities in the mean zonal wind (Maloney and Hartmann 2001; Maloney and Dickinson 2003; Serra et al. 2010; Crosbie and

Corresponding author e-mail: Yolande L. Serra, yserra@uw.edu

DOI: 10.1175/JCLI-D-16-0453.1

Serra 2014; Rydbeck and Maloney 2014; Molinari et al. 1997), interactions of the flow with topography (Mozer et al. 1996; Zehnder et al. 1999), and barotropic "breakdown" of the ITCZ (Wang and Magnusdottir 2005, 2006) also appear to play a role in wave growth in the eastern Pacific.

Evidence of thermodynamic controls supporting TD-wave activity is found in previous studies using both gridded observations (Hopsch et al. 2010; Rydbeck and Maloney 2014) and models (Caron et al. 2011; Caron and Jones 2012; Crosbie and Serra 2014; Roberts et al. 2015). Hopsch et al. (2010), Caron et al. (2011), and Caron and Jones (2012) highlight the importance of midlevel moisture ahead of TD-wave activity over Africa in supporting the waves as they propagate out over the Atlantic. Enhancement of column water vapor resulting from intraseasonal oscillations is also found to correlate well with a higher occurrence of TD waves and TC genesis in the eastern Pacific (Maloney and Esbensen 2003; Crosbie and Serra 2014). Roberts et al. (2015) additionally find that the number density of African easterly waves in their global model is sensitive to model horizontal resolution. While this result is attributed to a better representation of the African easterly jet in their model, it is also likely that higher resolution better captures the convection coupled to the waves. SST is also expected to play a role in favoring regions of convective activity through its influence on boundary layer moist entropy (Raymond 1995; Emanuel 1995; Raymond et al. 2003; Kuang 2008; Bretherton and Back 2009; Raymond et al. 2015). This idea is supported by Small et al. (2011), who use a regional model in the far-eastern Pacific to show that simulation of intraseasonal variability, also thought to share similarities with the "moisture mode" (Grabowski and Moncrieff 2004; Raymond and Fuchs 2007, 2009), is sensitive to the prescribed SSTs.

In addition to thermodynamic controls, another important factor in determining regions favorable for deep convection in the tropics, particularly TCs, is the presence of weak vertical shear (Gray 1968). The vertical structure of TD waves in the presence of varying background vertical wind shear across the tropical Pacific has been investigated in previous studies (Holton 1971; Reed and Recker 1971; Serra et al. 2008; Zhao et al. 2016). These studies suggest that central and eastern Pacific waves are typically found in regions where the background vertical shear is relatively weak ($<10\,\mathrm{m\,s^{-1}}$) (Holton 1971; Reed and Recker 1971; Serra et al. 2008). In contrast, in the western Pacific the vertical wind shear appears to impact the growth of the disturbances (e.g., Zhao et al. 2016), suggesting more complex energetics for the waves in this region. Where the waves are primarily sustained by a balance between convective heating and vertical motion, the wave circulations can be thought of as protecting the coupled convection from the environmental shear (Dunkerton et al. 2009). However, we might expect that at higher vertical shear this balance may be disrupted, resulting in a decay of the wave train in regions where convection plays a critical role in maintaining the waves (Maloney and Hartmann 2001; Maloney and Dickinson 2003; Serra et al. 2008, 2010; Crosbie and Serra 2014; Rydbeck and Maloney 2014), though modeling and case studies would be needed to test these ideas.

To examine the relationship between the combined environmental conditions discussed above and TD-wave activity we use the genesis potential index (GPI) of Emanuel and Nolan (2004). While the performance of genesis indices in climate models is highly variable (Camargo et al. 2007, 2014; Roberts et al. 2015; Camargo and Wing 2016), the genesis indices themselves are generally in good agreement among the models and are generally a good predictor of observed TC genesis frequency, suggesting the models are better able to capture the environment favorable to genesis than the TCs themselves (Camargo and Wing 2016). The representation of GPI in phase 5 of the Coupled Model Intercomparison Project (CMIP5) models used for the Intergovernmental Panel on Climate Change (IPCC) Fifth Assessment Report (AR5), as well as the environmental parameters comprising the index, has been examined previously with respect to cyclogenesis (Camargo 2013). However, this previous work focuses on global GPI and does not consider the covariability with TD-wave activity. By exploring the GPI–TD wave relationship in the models we hope to gain insight into model controls on TD waves in regions where the growth of such disturbances into TCs is supported in the gridded observations (e.g., Menkes et al. 2012).

An additional motivation for this study is the apparent southward shift in the TD wave track across the far-eastern Pacific region in the future climate seen in ECHAM5 (Roeckner et al. 2003), used for the IPCC AR4 (Bengtsson et al. 2006). This shift is also observed in CMIP5 models (Maloney et al. 2014). Using high-resolution model simulations based on the most aggressive CMIP5 warming scenario and a comparable tracking mechanism as in Bengtsson et al. (2006) and Maloney et al. (2014), Roberts et al. (2015) attribute shifts of eastern Pacific TC genesis toward the central Pacific to increased SST in this basin. While not specifically discussed in their study, a southward

TABLE 1. Summary of CMIP5 models used in this study along with the ensemble member identifiers and atmospheric (AGCM) and oceanic (OGCM) grid resolution. Ensemble members for CCSM4 are listed as historical, RCP4.5, and RCP8.5, respectively. Otherwise, the member was used for all three experiments. Grid resolution format is lon × lat grid points, L*n*, where *n* is the number of vertical levels. (Expansions of acronyms are available online at http://www.ametsoc.org/PubsAcronymList.)

Model	Code	Modeling group, country	Ensemble member	AGCM grid resolution	OGCM grid resolution
BCC_CSM1.1	BCC	Beijing Climate Center, China	r1i1p1	128 × 64, L26	360 × 232, L40
CanESM2	CAN	Canadian Centre for Climate Modelling and Analysis, Canada	r1i1p1	128 × 64, L35	256 × 192, L40
CCSM4	CCS	National Center for Atmospheric Research, United States	r1i1p1, r6i1p1, and r6i1p1	288 × 200, L26	384 × 320, L60
CNRM-CM5	CNR	Centre National de Recherches Météorologiques/Centre Européen de Recherche et Formation Avancée en Calcul Scientifique, France	r1i1p1	256 × 128, L31	362 × 292, L42
GFDL-ESM2M	GFM	NOAA/Geophysical Fluid Dynamics Laboratory, United States	r1i1p1	144 × 90, L24	360 × 200, L50
HadGEM2-ES	HGE	Met Office Hadley Centre, United Kingdom	r1i1p1	192 × 145, L38	360 × 216, L40
MIROC5	MI5	Atmosphere and Ocean Research Institute (The University of Tokyo), National Institute for Environmental Studies, and Japan Agency for Marine-Earth Science and Technology, Japan	r1i1p1	256 × 128, L40	256 × 224, L50
MPI-ESM-LR	MPI	Max Planck Institute for Meteorology, Germany	r1i1p1	192 × 96, L47	256 × 220, L40
MRI-CGCM3	MRI	Meteorological Research Institute, Japan	r1i1p1	320 × 160, L48	360 × 368, L51

shift in GPI and TC tracks in the far-eastern Pacific also appears in their study (Roberts et al. 2015, their Figs. 12 and 13). Here, we examine the environmental factors contributing to the southward shift in TD wave tracks, with a focus on the eastern Pacific, where shifts in the wave tracks have implications with respect to cyclogenesis through interactions of the flow with the topography of Central America (Zehnder et al. 1999; Molinari et al. 2000). A southward shift in these waves could also have implications for seasonal rainfall patterns over Central America, Mexico, and the southwestern United States (Amador et al. 2006; Adams and Stensrud 2007; Ladwig and Stensrud 2009; Seastrand et al. 2015).

The first part of this study assesses the representation of easterly waves across the IAS and far-eastern Pacific in CMIP5 models through their ability to capture synoptic-wave track density and mean strength based on low-level relative vorticity. A second independent wave activity metric based on outgoing longwave radiation (OLR) is also used to assess the location and relative strength of the convective coupling to the waves in the models. In the second part of this study we examine the environmental factors associated with the projected shift in TD wave tracks in the future climate across the region. Initial results of this study documenting the model historical track biases and the projected southward shift of the multimodel ensemble mean wave track density also appear in the National Oceanic and Atmospheric Administration's Modeling, Analysis and Prediction Program (MAPP) synthesis papers on North American climate in the CMIP5 models (Sheffield et al. 2013; Maloney et al. 2014).

2. Data

We selected nine CMIP5 models for the analyses in this study (Table 1), using one ensemble member from each model and no more than one model from a given modeling center in order to maximize the independence of our model subset for our multimodel ensemble (MME) statistics. The nine models considered here provide a good spread in the geographic location of the modeling centers and the available horizontal resolution

for the models participating in CMIP5 (Table 1). We chose the May–November 1979–2005 time period (27 years) for the historical period analysis to coincide with the assimilation of satellite observations, which are essential in the data-sparse eastern Pacific. For the future analysis we focus on May–November 2070–99. The future time period covers the last 30 years of the CMIP5 future projection experiments and thus provides the upper bounds on model responses to the given warming scenario. The representative concentration pathway 4.5 and 8.5 (RCP4.5 and RCP8.5) model experiments are compared with the historical model experiment. RCP4.5 is an intermediate emissions scenario, which stabilizes to a radiative forcing of 4.5 $W m^{-2}$ after about 2070, while RCP8.5 steadily increases to a more aggressive forcing of 8.5 $W m^{-2}$ by 2100 (Moss et al. 2010). We focus most of our discussion on RCP8.5 results, as the RCP4.5 results are generally similar but of smaller magnitude.

Model representation of the tropical TD wave track and the background environment in the IAS and eastern Pacific within which the track is embedded is evaluated using observations and reanalysis. NOAA/National Climatic Data Center (NCDC) interpolated OLR is available from the Earth System Research Laboratory at 2.5° × 2.5° horizontal resolution and daily time resolution from 1974 to the present (Liebmann and Smith 1996). These data are abbreviated as CDC OLR throughout the text and figures. The observed SST used by this study is the HadISST, version 1.1, 1° gridded monthly SST product provided by the Met Office Hadley Centre and covers the period from 1870 to the present (Rayner et al. 2003). The Kaplan SLP data, available from January 1854 to July 2001, are provided by the NOAA/OAR/ESRL Physical Sciences Division (PSD), Boulder, Colorado, from their website (http://www.esrl.noaa.gov/psd/gcos_wgsp/Gridded/data.kaplan_slp.html) (Basnett and Parker 1997). For winds and relative vorticity we rely on ERA-Interim (ERAI) fields obtained from the ECMWF data server at 1.5° × 1.5° horizontal resolution and 6-hourly time resolution. ERAI reanalysis fields are produced on a native spectral T255 resolution horizontal grid using four-dimensional variational (4D-Var) data assimilation every 12 h (Dee et al. 2011). This reanalysis product is selected for its improved representation of the tropics over previous-generation reanalysis products, particularly with respect to tropical moisture (Dee et al. 2011).

3. Methodology

We employ two methods to isolate TD-wave activity: the vorticity tracking method of Hodges (1995, 1999), from which we obtain track density (TDEN) and mean track strength (MSTR), and the TD-filtered OLR method of Wheeler and Kiladis (1999), which provides a measure of TD-wave activity that is independent of the vorticity tracking method. We compare model TDEN, MSTR, and TD-filtered OLR to observations and also examine the spatial relationships between this activity and specific environmental variables and indexes that are expected to influence wave activity through favoring or disfavoring convection coupled to the waves (Sobel et al. 2001; Raymond and Fuchs 2007; Raymond et al. 2015). This approach reveals why certain models may fail to reproduce TD-wave statistics seen in observations, because of a poor representation of the environment favoring wave activity or displacement of favorable wave activity zones. These results provide valuable information when assessing the projected change to the TD-wave activity in future model experiments. The environmental indexes and variables examined include GPI, SST, 200–850-hPa wind shear (WSH), 700-hPa specific humidity (q700), and the Pacific Walker index (PWI). OLR is also used to assess each model's overall deep convective regions and the relative fraction of intraseasonal variance attributable to TD waves in each of the models.

a. Vorticity tracking

TD waves are tracked based on the method of Hodges (1995, 1999) using 6-hourly, 850-hPa relative vorticity from the nine CMIP5 models listed in Table 1 for May through November 1979–2005. The 850-hPa level is chosen as it is standard output from all of the modeling centers that provide the 6-hourly data product used for this study. These tracks are compared with those from ERAI for the same period. Both model and reanalysis have been smoothed with a spectral T42 Gaussian spatial filter prior to calculating relative vorticity and tracking vorticity maxima to better capture the synoptic features of the vorticity field and to obtain comparable relative vorticity fields across models of differing spatial resolution. Disturbances in the smoothed fields that exceed a strength threshold of $+0.5 \times 10^{-5} s^{-1}$, persist for at least 2 days, and have tracks of at least 1000 km in length are tracked. This method primarily identifies westward-moving disturbances having characteristics consistent with those of TD waves (Serra et al. 2010), although tropical storms including cyclones are not excluded. The resulting tracks are then used to obtain TDEN, defined as the number of tracks within a 5° spherical cap per month, and MSTR, defined as the mean 850-hPa vorticity along the tracks contained within each 5° spherical cap. For a more complete description of this method as it is applied to ERAI in the tropical eastern Pacific, as well as the method's potential shortcomings, the reader is referred to Serra et al. (2010).

Of interest to this study is Serra et al.'s (2010) discussion of the difficulty in tracking vorticity maxima over Central America, particularly at 850 hPa. As a consequence, the present study does not attempt to evaluate track genesis density in the eastern Pacific, although in principle, this would be of great interest given the implications for wave initiation mechanisms in this region in the models.

b. TD-filtered OLR

Convection coupled to TD waves is isolated through space–time filtering of OLR following the method of Wheeler and Kiladis (1999), which we have previously applied to satellite observations in the tropical eastern Pacific (Serra et al. 2008, 2010). The space–time filter used for this study selects for 2–7-day westward-propagating disturbances with global (zonal) wavenumbers between 6 and 16 using NOAA daily OLR fields from 1979 to 2005. May through November is then extracted from the filtered dataset for each year. This analysis is independent of the relative vorticity tracking method described above and thus provides an independent measure of TD wave tracks across the region.

c. Environmental indices

A full discussion of the calculation of GPI is given in Camargo et al. (2007). As in that study, we obtained code (from ftp://texmex.mit.edu/pub/emanuel/TCMAX/) to calculate the potential intensity (PI) and then obtain the GPI using the following formulation:

$$\mathrm{GPI} = |\eta 10^5| \left(\frac{\mathrm{RH}}{50}\right)^3 \left(\frac{\mathrm{PI}}{70}\right)^3 (1 + 0.1 \times \mathrm{WSH})^{-2},$$

where η is 850-hPa absolute vorticity, WSH is the 200–850-hPa wind shear, and RH is 700-hPa relative humidity. The calculation of the PI depends on SST, sea level pressure, and the vertical profiles of temperature and moisture. For the nine CMIP5 models and ERAI, track parameters show similar cross correlations with PI as SST so the PI fields are not reproduced here. Details on the PI parameter in CMIP5 models and how it changes in the future have been addressed elsewhere (Camargo 2013; Emanuel 2013; Ting et al. 2015). In addition, as TDEN and MSTR are indirect measures of low-level vorticity in the models and reanalysis, we do not separately examine 850-hPa absolute vorticity. Our analysis does suggest that changes in absolute vorticity in the future (RCP4.5 and RCP8.5) do correspond to changes in track density, but given the close relationship between the two it is difficult to separate cause and effect for this result. Significant changes in this parameter are also only present in five (one) out of nine models for RCP8.5 (RCP4.5).

To investigate how the PWI might be impacting CMIP5 model biases in WSH, we calculate a PWI following the method of Vecchi et al. (2006), where the difference in SLP between the central-eastern Pacific and Indian Ocean–western Pacific is calculated from Kaplan monthly SLP anomalies with respect to the historical period used for this study. The index is then averaged over the May through November period each year for all datasets. The Kaplan SLP data are used as the observational dataset to be consistent with the previous studies of Vecchi et al. (2006) and Vecchi and Soden (2007). As Kaplan SLP data are only available through July 2001, we used 1974–2000 to compare with the CMIP5 model historical period (1979–2005). However, similar results are obtained when the models are compared to the PWI based on ERAI SLP for the 1979–2005 time period (not shown).

d. Model evaluation

Comparisons of CMIP5 model fields with reanalysis and gridded observations are done primarily using bias plots, where the bias is defined as the model minus the observations or reanalysis. Difference plots are constructed in a similar way but are used to compare the model historical and future periods, where in this case the difference is defined as the future minus historical values. Taylor diagrams (Taylor 2001) are also used to assess the agreement between the models and observation-based fields. The model and observation-based fields are regridded to a 128 × 64 longitude–latitude grid points, shared by the BCC and CAN models, to permit comparisons on a model grid scale. Regridded model fields are also used for the calculation of the MME mean for the historical and future periods.

4. Results

a. Representation of TD-wave activity during the historical period

1) Vorticity-track statistics

The TDEN and MSTR for ERAI and the MME are shown in Fig. 1. Overlaid on the ERAI TDEN in Fig. 1a is the 25th-percentile observed May–November 1979–2005 OLR contour. Figure 1 indicates that the vorticity tracking captures disturbances traveling along the axis of minimum OLR or maximum deep convection in the eastern Pacific, with a maximum density along the west coast of Mexico near the center of the OLR minimum.

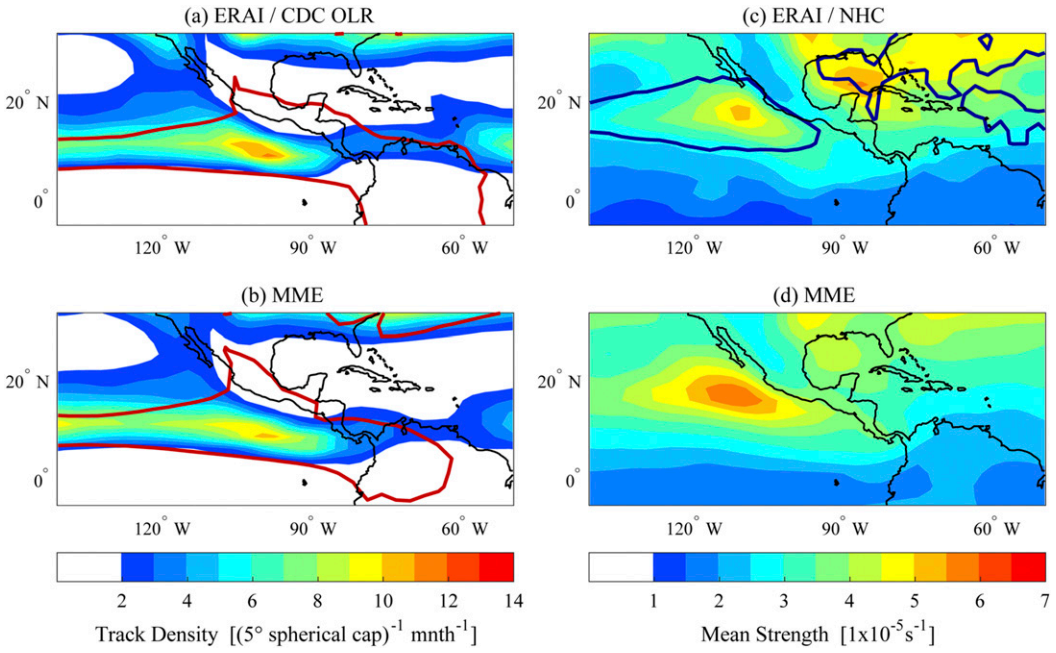

FIG. 1. Track density at 850 hPa (shaded contours) based on data from (a) ERAI and NOAA CDC and (b) the MME for the May–November 1979–2005 period. The 25th-percentile OLR contour is shown in (a) and (b) for CDC OLR (242 W m^{-2}) and the MME (246 W m^{-2}), respectively. (c),(d) As in (a),(b), but for track mean strength at 850 hPa. The NHC best-track tropical storm density 0.5 counts per day contour is also shown in (c) for reference.

Figure 1b is similar to Fig. 1a but for the MME. Like the reanalysis, the MME TDEN lies within the region of minimum OLR for the models, except in the western Atlantic where the MME 25th-percentile OLR contour does not extend and the MME TDEN is less than in the reanalysis. The MME 25th-percentile OLR contour also indicates that the models have less deep convection along the east coasts of Central America and southern Mexico. MME TDEN strongly underestimates the peak of activity in the far-eastern ITCZ, while it overestimates wave activity farther west within the ITCZ. Overall, however, the models capture the strong connection between the synoptic wave activity and the mean ITCZ seen with the reanalysis and satellite observations.

Figure 1c shows ERAI MSTR overlaid with tropical cyclone track density for the May–November 1979–2005 seasons. The tropical cyclone track density is obtained from the National Hurricane Center's (NHC) best-track data archive. Unlike the MSTR in Fig. 1a, the NHC track density represents the density of systems that reached tropical storm strength (34 kt; 1 kt $\approx$ 0.51 m s^{-1}) or greater and were followed by the NHC. The geographical distribution of the maximum in MSTR in the eastern Pacific is shifted north of the maximum in TDEN, following more closely the maximum in NHC track density. Thus, while high TDEN is primarily associated with disturbances along the ITCZ, the envelope of high MSTR is shifted toward the locations of tropical cyclones.

The MME MSTR statistics (Fig. 1d) indicate a tendency for models to somewhat overestimate the strength of disturbances in the eastern Pacific and significantly underestimate the strength of the disturbances along the southeast coast of the United States and over the Gulf of Mexico as compared to ERAI. On the other hand, the MME envelope of MSTR is in a similar location as the envelope of NHC best-track data in the eastern Pacific and is in agreement with ERAI. An attempt to estimate TC frequency in the CMIP5 models is beyond the scope of this study. However, such analyses have been presented elsewhere (Camargo 2013; Camargo and Wing 2016).

Examining the individual CMIP5 TDEN statistics for the historical period in Fig. 2, it is apparent that BCC, CAN, CCS, and MRI overestimate the number of tracks from across northern South America into the eastern Pacific and suggest more longitudinally oriented tracks shifted south from what is observed in the reanalysis across this region. MI5 also suggests a weak southward shift but only in the far-eastern Pacific. In contrast to these results, GFM, HGE, MI5, and MPI tend to

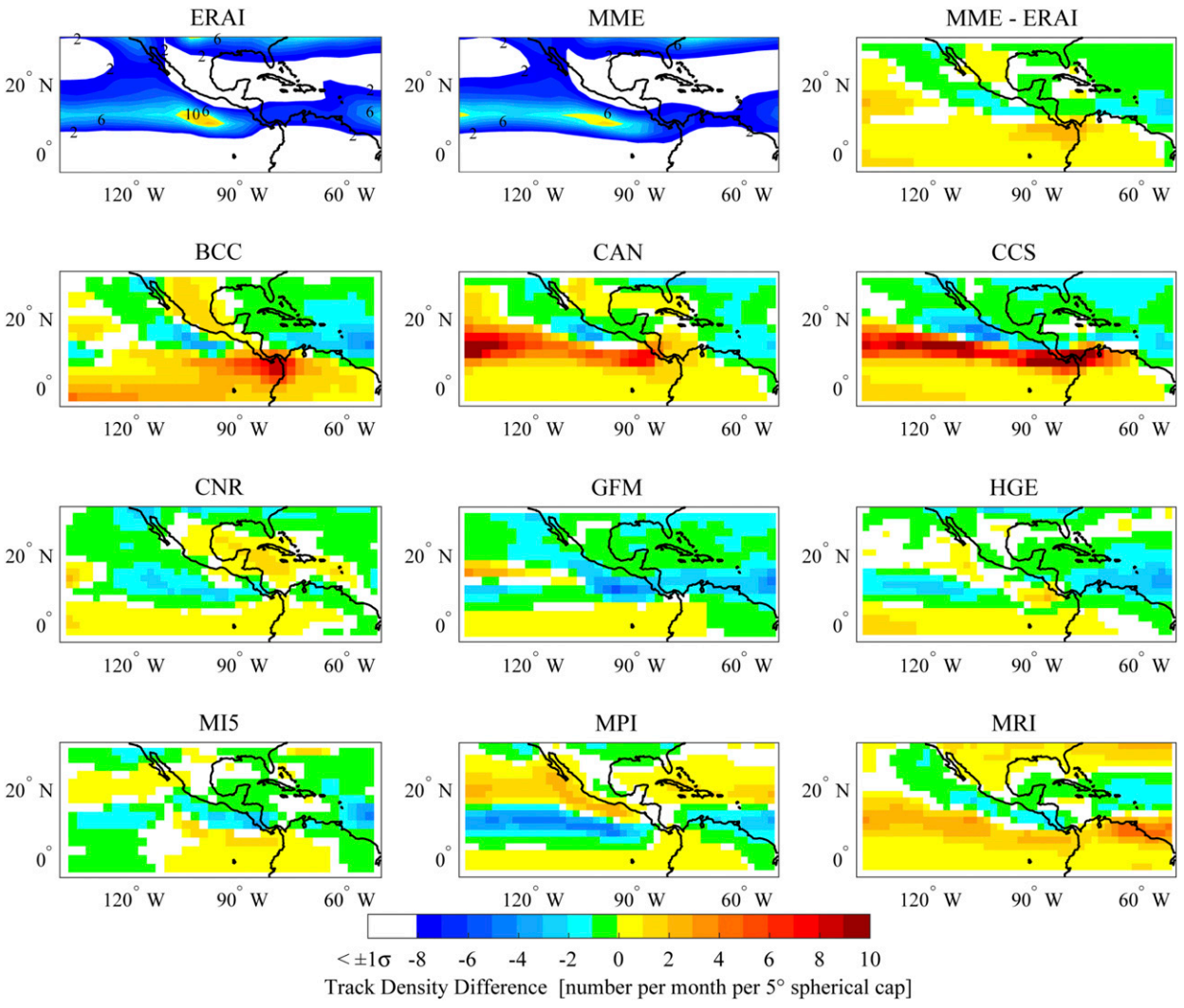

FIG. 2. Track density at 850 hPa in (top left) ERAI, (top center) multimodel mean, and (top right) their difference for the historical period. The remaining panels are differences for individual models with respect to ERAI. Only differences that exceed one standard deviation of the mean based on the individual model or MME are shown. Shaded contour interval is 1 count per month per 5° spherical cap in all panels.

underestimate the TDEN across the ITCZ. Of these, MPI shifts the track northward in both the western Atlantic and the eastern Pacific, while GFM shifts it northward only in the far-western portion of the domain. Of these nine models, CNR, HGE, and MI5 have the smallest biases across the region. The MME somewhat cancels the individual biases seen here, with an overall underestimate of tracks off the east coast of Brazil and along the west coast of Central America and Mexico and a small overestimate of tracks off the west coast of Colombia and in the central Pacific. Unlike TDEN, the model biases in MSTR shown in Fig. 3 are generally consistent among the models and, as stated above, indicate a tendency to underestimate the strength of disturbances in the western Atlantic and Gulf of Mexico and overestimate the strength of disturbances in the eastern Pacific.

Figure 4 shows the Taylor diagrams for the TDEN and MSTR. Taylor diagrams show the standard deviation, RMSE, and correlation statistics all on one diagram. The best models will fall closest to the reanalysis point where the RMSE approaches zero, the standard deviation approaches that of the reanalysis, and the correlation approaches one. Consistent with the bias plots (Fig. 2), the best overall agreement between model TDEN and reanalysis is seen for CNR, MI5, HGE, and GFM, with the MME slightly outperforming any individual model (Fig. 4a). The high spatial correlation

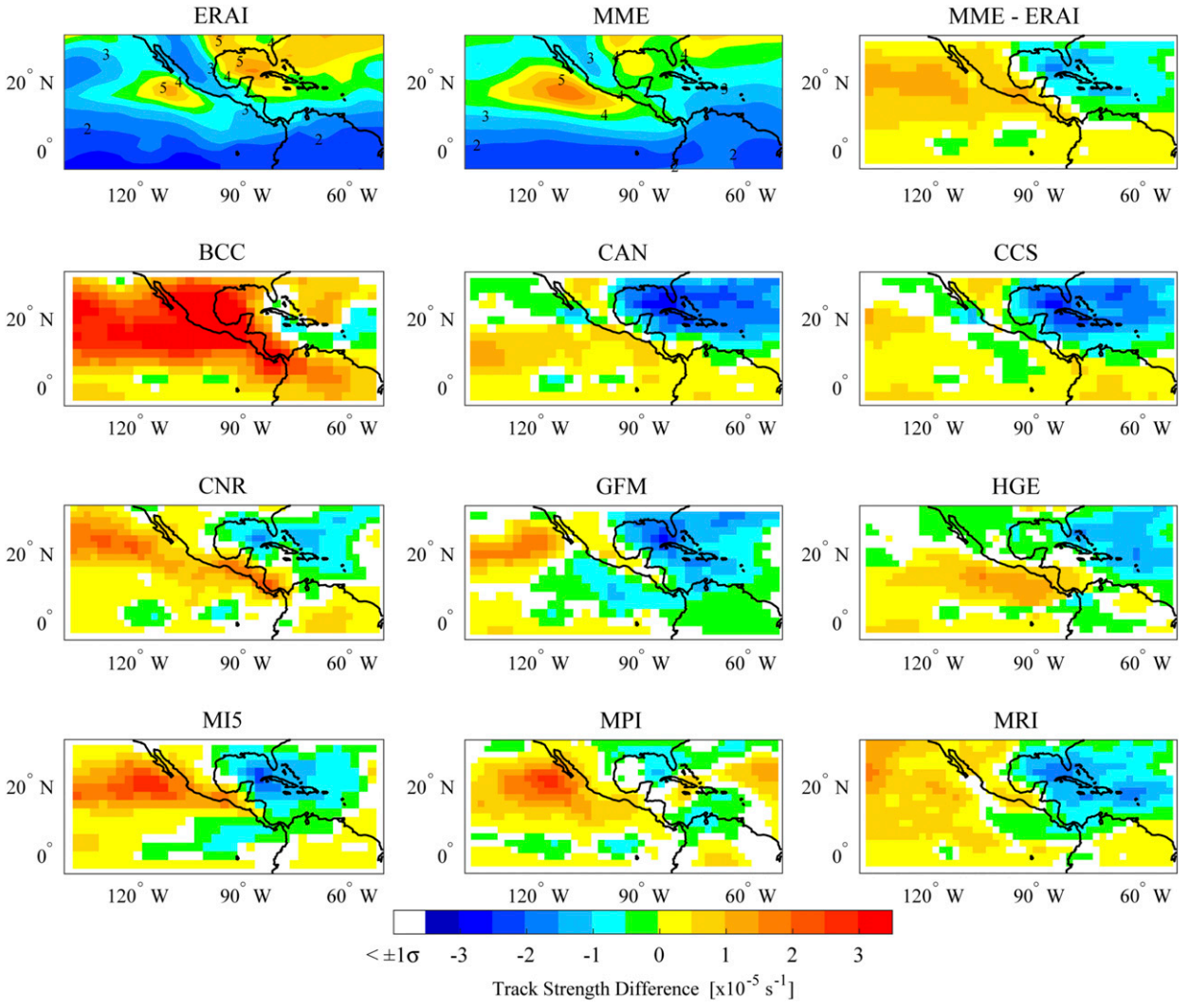

FIG. 3. As in Fig. 2, but for vorticity-track mean strength. Shaded contour interval is $0.5 \times 10^{-5}\,s^{-1}$ in all panels.

(near 0.9) for these models and their small RMSEs relative to the standard deviation in the reanalysis suggests these models in particular are capturing the number density of TD waves in the right location across the ITCZ.

The MSTR shows poorer agreement with reanalysis than TDEN, with all but one spatial correlation at or below 0.7 (Fig. 4b). The best agreement for MSTR is seen for CNR, HGE, GFM, MRI, and MPI, with the MME showing comparable statistics to the individual models. The lower spatial correlations compared to TDEN and RMSEs of similar magnitude to the standard deviation for this parameter gives less confidence in the model's ability to capture MSTR than TDEN. This is consistent with the fact that MSTR is more a function of the model's ability to capture subgrid-scale processes including tropical storms and hurricanes.

Overall, the TD-wave statistics (both number density and strength) are best captured by CNR, HGE, and GFM in comparison to ERAI.

2) TD WAVES IN OLR

As discussed in section 3c, in addition to using the vorticity tracking method, we also use TD-filtered OLR, which provides a second and independent measure of the TD-wave activity across the region. Before considering the space–time-filtered field we first examine model representation of deep convection across the ITCZ region (Fig. 5). Biases in model OLR are most pronounced over land, where the MME underestimates the depth of the convection particularly over Central and South America, likely in part because of the inability of the models to resolve deep convection initiated over the steep terrain in these regions. Focusing on the

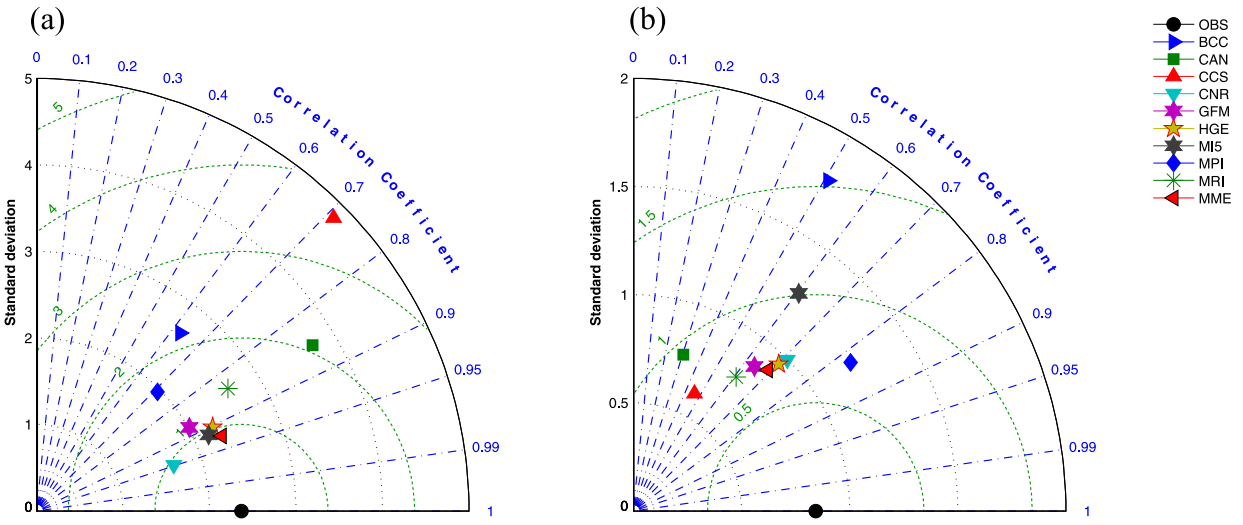

FIG. 4. Taylor diagrams of (a) vorticity-track density and (b) vorticity-track strength for the IAS region (2.5°–25.0°N, 130°–50°W). Models are compared to ERAI vorticity-track statistics.

individual models, the underestimate of mean deep convective activity over Central and South America is seen in all but the MRI model, with the largest biases seen in CAN and GFM, two of the lowest-resolution models (Table 1). These biases are discussed in detail in Yin et al. (2012). Individual models also both underestimate (BCC, CCS, CNR, and HGE) and overestimate (CAN) total activity in the ITCZ, while others (CNR and MI5) place too much deep convection south of the observed ITCZ. As for the MME, the biases over land exceed those over ocean, with differences over ocean generally within $\pm 10\,\mathrm{W\,m^{-2}}$.

Examining TD-filtered OLR (Fig. 6), regions of positive (negative) TD-filtered OLR variance biases in the models correspond to positive (negative) biases in TDEN (Fig. 2). And as with TDEN biases, there is little agreement among the models regarding the sign of the biases in TD-filtered OLR variance across the IAS and eastern Pacific, with about half underestimating TD-wave variance (BCC, GFM, HGE, and MI5) while a similar number overestimate it (CCS, CNR, MPI, and MRI). This result differs from that for CMIP3, for which the majority of models were found to underestimate the magnitude of TD-wave activity in the eastern Pacific ITCZ (Lin et al. 2008). The MME differences indicate that the models as a whole have difficulty suppressing convection on synoptic scales in the suppressed regions of the domain, which include the equatorial eastern Pacific, subtropical eastern Pacific off the west coast of the United States, and the equatorial Atlantic off the east coast of Brazil. The regions and sign of the biases in TD-wave convective activity in the models and MME do not generally coincide with the regions and sign of biases in mean OLR (Fig. 5). This emphasizes that model biases in convective activity are scale dependent and that a model's ability to capture the mean OLR implies little about its ability to capture synoptic variability. This result is also seen in spectral analyses of tropical intraseasonal modes in rainfall for CMIP3 and CMIP5 (Lin et al. 2008; Hung et al. 2013; Jiang et al. 2013). As the TD-filtered OLR biases closely coincide with TDEN biases in the models, such biases in TD-wave activity are not simply related to a model's convective parameterization but are also linked to biases in low-level vorticity.

Model TD-wave activity, as measured using TD-filtered OLR, is also evaluated using a Taylor diagram in Fig. 7. The spatial correlation of the model TD-filtered OLR standard deviation generally lies above 0.7 and RMSEs are all less than the standard deviation for this parameter, suggesting that individual model wave convective activity is reasonably well positioned with respect to the observations and of similar magnitude. However, there is a large spread in model variability in this activity compared to the observed variability. As a result, the MME shows the best overall agreement with the observations, with no models clustering around the MME.

b. Relationship of TD-wave activity to the environment

1) GEOGRAPHIC DISTRIBUTION OF ENVIRONMENTAL PARAMETERS AND THEIR BIASES

To better understand how environmental factors are impacting each model's representation of TD-wave

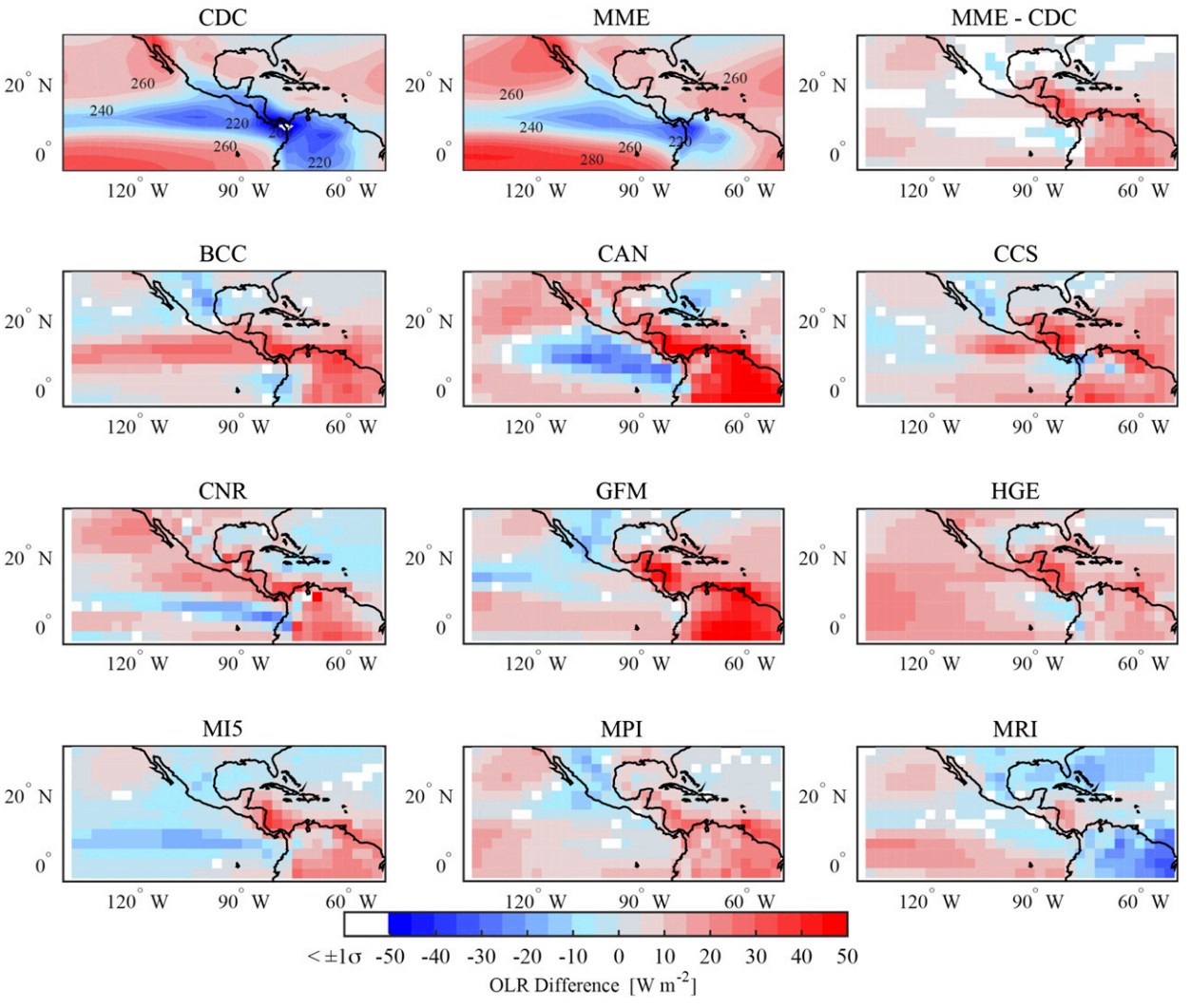

FIG. 5. As in Fig. 2, but for OLR. Model fields are compared with CDC OLR. Shaded contour interval is 5 W m^{-2} in all panels.

activity, we examine the spatial distribution of the biases in the relevant fields and their relationship to the biases in TDEN and MSTR. This information is important for both understanding model deficiencies and interpreting future projections in TD-wave activity. While CMIP5 SST biases have been reported elsewhere (Kozar and Misra 2013; Camargo 2013), model TD-wave activity is sensitive to this parameter so we reproduce these biases here for the models used in this study. Similarly, GPI in CMIP5 (Camargo 2013) and ERAI (Jiang et al. 2012) has been studied elsewhere, but the strong correspondence between this field and TD waves has not been previously investigated.

SST can affect the strength of convection coupled to TD waves through its impact on atmospheric stability, moist entropy fluxes, and boundary layer moisture. More intense convection coupled to the waves feeds back on the wave circulations and thus on vorticity-track density (more waves reaching the threshold for tracking) and mean strength (Serra et al. 2008; 2010; Rydbeck et al. 2013). Figure 8 is constructed like Fig. 2 but shows May–November 1979–2005 HadISST, the MME SST, and individual model biases for differences greater than one standard deviation of the mean for the model or MME. The SST biases shown are in agreement with previous studies (Camargo 2013; Kozar and Misra 2013) and suggest there is a tendency for all models to underestimate SST in the eastern portion of the domain, especially within the region of maximum wave strength (10°–20°N) where systems generally intensify. MPI shows the smallest negative bias in the western Atlantic and Gulf of Mexico and also shows the best agreement with ERAI MSTR in these regions (Fig. 3). Similarly, the overestimation of SST in the eastern Pacific along

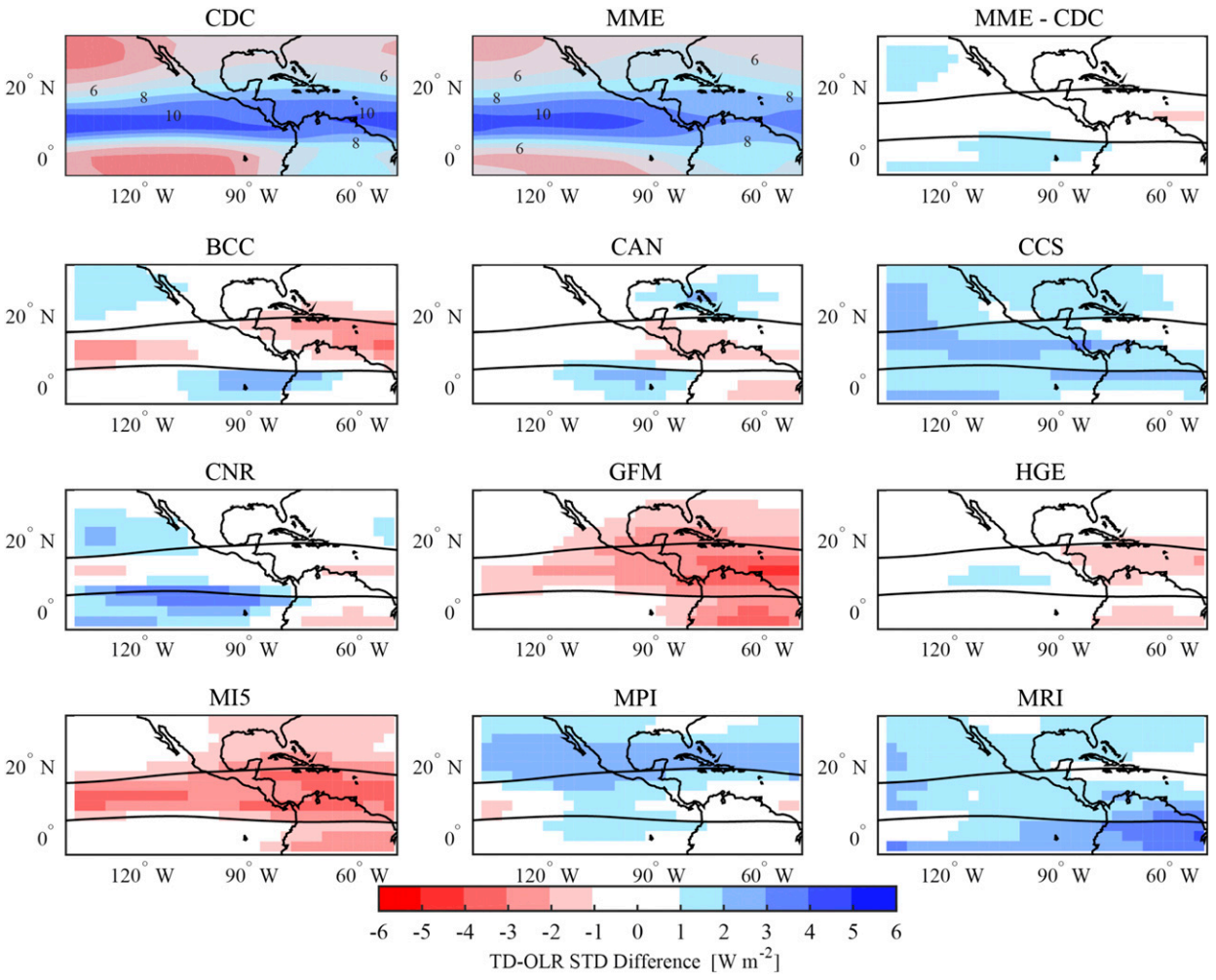

FIG. 6. As in Fig. 2, but for TD-filtered OLR. Shaded contour interval is 2 W m^{-2} in mean fields at (top left) and (top center) and 1 W m^{-2} in the difference fields. Also shown is the 8 W m^{-2} contour taken from (top left) in the difference fields for reference.

the west coast of Mexico and north of 10°N in many models corresponds to an overestimation of MSTR in this basin. An exception is HGE, which indicates a small positive bias in MSTR in the eastern Pacific but a small negative bias in SST in this region. The correspondence of biases in SST to biases in TDEN is less evident, although the largest negative biases in SST do correspond to negative biases in TDEN in both the MME and individual models.

As discussed in the introduction, another potentially important factor in determining regions favorable to eastern Pacific TD waves is the presence of weak vertical shear (Holton 1971; Reed and Recker 1971; Serra et al. 2008). The WSH for the ERAI and MME are shown in Fig. 9, along with the individual model biases. The geographic distribution of the MME shear is similar to the reanalysis across the region but with somewhat higher values everywhere except along about 10°N in the eastern Pacific. Examination of the biases in the 850- and 200-hPa zonal winds indicates that the positive biases over the equatorial eastern Pacific are primarily the result of biases in the low-level winds, while biases north of 10°N in this basin primarily result from biases in the upper-level winds (not shown). The transition region near 10°N shows good agreement with ERAI. The positive biases in WSH seen over the Caribbean Sea–western Atlantic and eastern Pacific north of 10°N, where the MME WSH is mostly at or above 10 m s^{-1}, correspond to negative biases in the MME TDEN (Fig. 2). However, where MME WSH is below about 10 m s^{-1}, MME TDEN biases do not appear to correspond to WSH biases. Similarly, the pocket of low shear off the South American–Panamanian west coast in the far-eastern Pacific corresponds to a positive bias in the MME TDEN (Fig. 2). As there is no bias in WSH at this

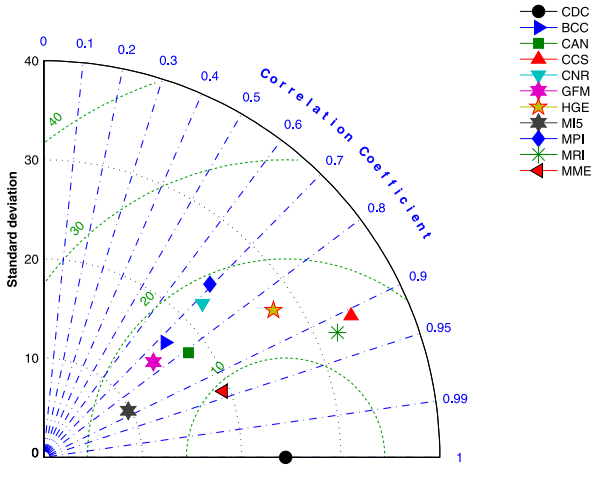

FIG. 7. Taylor diagram of the standard deviation in TD-filtered OLR for the IAS region (2.5°–25.0°N, 130°–50°W). Models are compared to the CDC TD-filtered OLR.

location, the TDEN bias is related to some other factor(s) in the models; however, the low WSH is at least supporting the higher MME TDEN.

This relationship between WSH and TDEN biases is also seen in the individual models. For instance, CAN has large positive biases in WSH across the eastern Pacific north of about 15°N and negative biases south of this region (Fig. 9). These biases correspond to negative (positive) TDEN biases north (south) of 15°N for this model (Fig. 2). The large WSH bias for CAN in the eastern Pacific likely also contributes to the more longitudinal TDEN found in this model. A similar relationship between WSH and TDEN biases is seen for CCS and MRI. In contrast, MPI WSH biases are positive south of about 15°N and negative north of this region, corresponding to a northward shift of the TDEN for this model. While the MME WSH showed no significant bias off the South American–Panamanian west coast, a low bias is seen in HGE and MRI in this region, corresponding to a positive bias in TDEN there. These results imply that TD waves are not favored in areas of high vertical wind shear, although the exact mechanisms by which the shear interacts with the waves are unclear.

It has been suggested that variability in the vertical wind shear in the tropical western Atlantic is related to variability in the Pacific Walker cell circulations, with larger shear associated with weaker Walker circulations (Vecchi and Soden 2007). To better understand how biases in WSH over the region might be related to biases in PWI for the nine models examined in this study, we plot these biases for the individual models in Fig. 10a. WSH biases are calculated based on monthly differences between the model and ERAI averaged over the region 10°–25°N, 120°–60°W. The biases in WSH tend to be negatively correlated with the biases in the PWI for the models; however, this relationship has a relatively low correlation (−0.26). While the bias in the Pacific Walker cell may be a contributing factor to the bias in WSH, and thus to the bias in TDEN, this circulation does not appear to be a consistent predictor of WSH in the individual models for the historical period. This result changes for the future climate scenarios, as will be discussed below.

In addition to SST and WSH, midlevel moisture plays a significant role in the coupling of convection to modes of tropical intraseasonal variability, including TD waves (Raymond and Fuchs 2007; Kuang 2011; Yasunaga and Mapes 2012; Kim et al. 2014; Raymond et al. 2015). Figure 11 shows the 700-hPa specific humidity comparisons for the historical period with the same format as in Fig. 2. Midlevel moisture is a maximum along the axis of the ITCZ where TDEN (Fig. 2), mean high cloudiness (Fig. 5), and TD-filtered OLR variance (Fig. 6) are also a maximum. Also evident is the peak in moisture into northwestern Mexico and the southwestern United States as part of the North American monsoon. The MME has an overall dry bias in midlevel moisture compared to ERAI, with the driest biases observed over the Caribbean Sea, over the Gulf of Mexico, and across the ITCZ. This pattern is relatively consistent across individual models, with the dry region over the Caribbean Sea being the most consistent. Over the May through November period 850-hPa height biases shift from being largest over the Pacific sector in June to being largest over the western Atlantic sector during October and November (not shown). The strength of the North Atlantic subtropical high (NASH) is strongly influenced by Atlantic SST structure. In particular, a large (small) Western Hemisphere warm pool weakens (strengthens) the NASH over the western Atlantic (Wang et al. 2007). The negative SST biases in the western Atlantic shown in Fig. 8 are thus consistent with the positive height biases and corresponding dry midtroposphere in these models. Positive NASH biases in CMIP3 have also been reported (Li et al. 2012).

There is notable correspondence between the region of midlevel moisture bias in the MME and TDEN biases, with the dry (moist) regions coincident with negative (positive) TDEN. Similarly, there is a positive bias in TD-filtered OLR variance in the MME off the west coast of South America (Fig. 6) where the moist bias in midlevel moisture resides. Dry biases in midlevel moisture over the ITCZ also correspond to negative biases in model deep convection, except for CAN off the west coast of Central America.

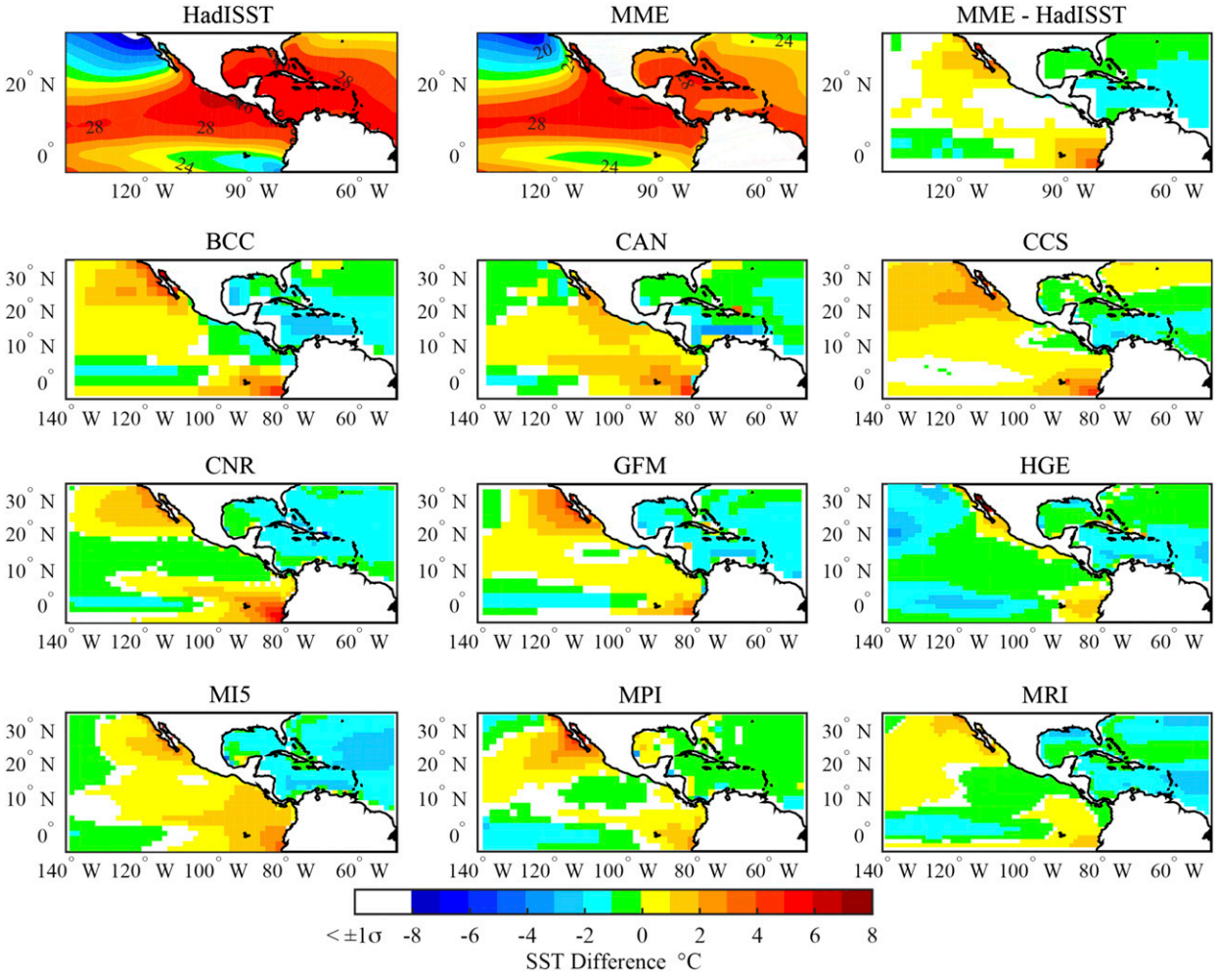

FIG. 8. As in Fig. 2, but for SST. Model fields are compared with HadISST. Shaded contour interval is 2°C for the mean fields and 1°C for the difference fields.

The above discussion suggests that several factors contribute to the distribution of TDEN and MSTR across the IAS and eastern Pacific, as well as to their biases in the CMIP5 models. Through the use of the GPI we attempt to understand the combined impact of several environmental factors on TD wave mean fields and biases in the models where such disturbances tend to intensify in observations (e.g., Camargo et al. 2007). We find that GPI is underestimated in nearly all of the models (Fig. 12), especially along the west coast of Central America and Mexico and over the western Caribbean Sea and Gulf of Mexico. Examination of biases in model absolute vorticity (not shown) suggests that the GPI biases near the coasts in this region result from topographic effects, as has been suggested previously (Vitart et al. 1997; Camargo et al. 2005). Several models extend the negative bias into the western Atlantic (BCC, CAN, CCS, HGE, and MRI) and eastern Pacific (BCC, CNR, and HGE) ITCZ. The exceptions are MI5 and MPI, which show positive biases in the eastern Pacific, with MPI additionally showing a positive bias over the Caribbean Sea and western Atlantic. These biases tend not to be associated with biases in absolute vorticity (not shown). The GPI model biases reported here are in contrast to Camargo (2013) likely because of the negative midlevel moisture bias in the National Centers for Environmental Prediction (NCEP) Reanalysis-1 used for comparison with CMIP5 models in that study (Camargo 2013). In agreement with the results in Fig. 12, Walsh et al. (2013) note a negative bias in GPI for CMIP3 models using ERA-40 but a positive bias using NCEP Reanalysis-2, which is also attributed to low midlevel moisture in the NCEP product. ERAI is expected to have improved representation of tropical moisture over both these products (Dee et al. 2011).

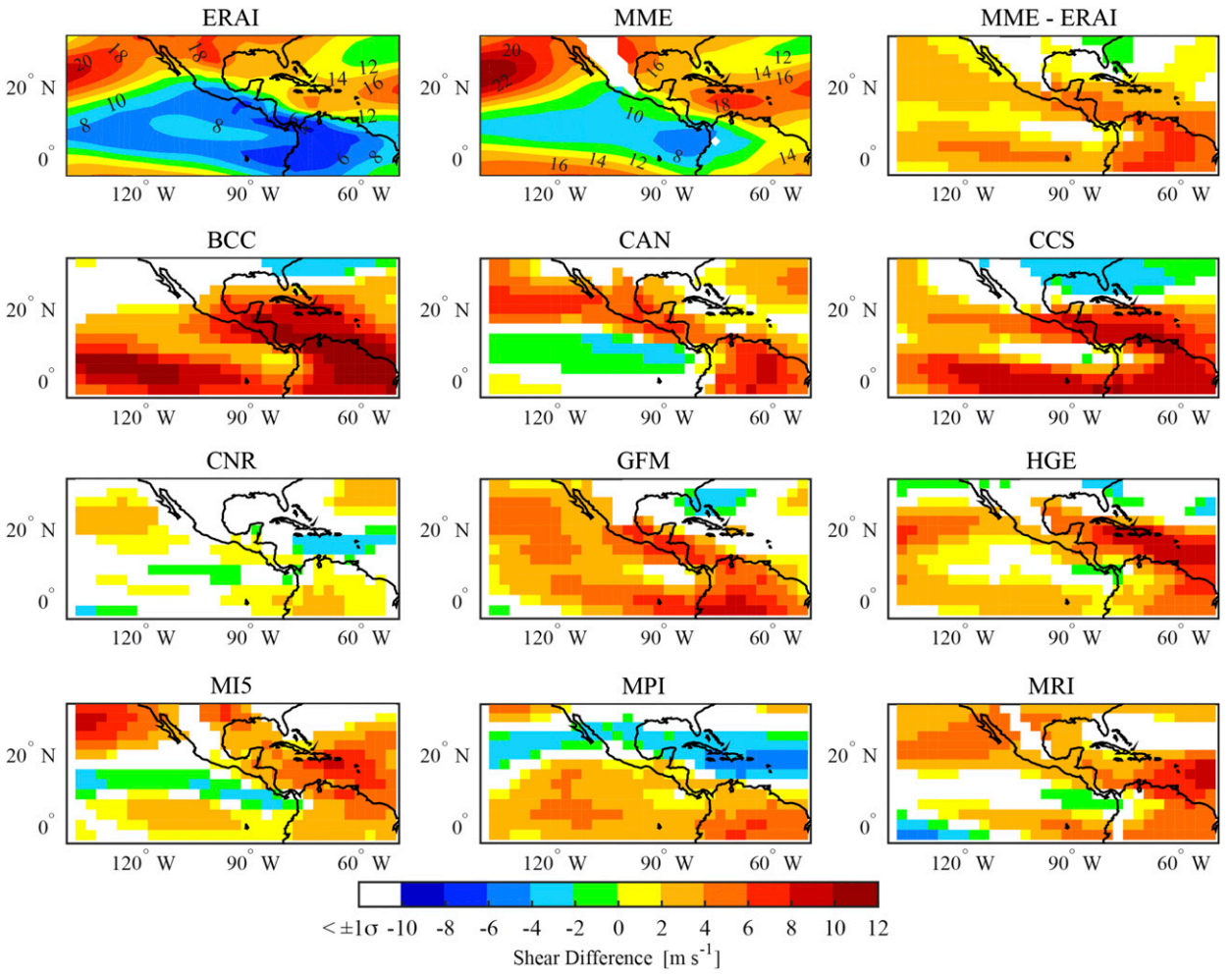

FIG. 9. As in Fig. 2, but for WSH. Shaded contour interval is 2 m s^{-1}.

Areas of high GPI in ERAI generally correspond to areas of high ERAI TDEN and TD-filtered OLR variance, with maxima in GPI off the coast of Mexico and the southeastern United States corresponding to maxima in ERAI MSTR. While the calculation of GPI includes absolute vorticity from ERAI, and is therefore not entirely independent from the vorticity-track parameters, this result suggests that GPI highlights areas favorable for TD-wave activity. The CMIP5 models also show a correspondence between track parameters, TD-filtered OLR variance, and GPI, but with weaker maxima in GPI as discussed above. These results are consistent with the results for CMIP3 models for the Atlantic, where model GPI in the Atlantic main development region (MDR) is well correlated with African easterly wave activity over this region (Daloz et al. 2012). Additionally, Caron and Jones (2012) find that GPI in the MDR is well correlated with African easterly wave activity upstream over the Sahel through wave modulation of both the large-scale shear and midlevel moisture in regional model simulations.

2) QUANTIFYING THE RELATIVE IMPORTANCE OF ENVIRONMENTAL FACTORS IN TD-WAVE ACTIVITY

To objectively quantify the relative importance of the above environmental factors in determining wave activity in the models and in observations, we examine the spatial cross correlations between the track parameters and the key environmental fields for the historical period in observations and the MME, as well as the spatial cross correlations between the MME biases in these parameters (Table 2). The spatial cross correlations are calculated over the region 0°–25°N, 125°–50°W, which encompasses the main wave train across the IAS and the main area of TC genesis in the eastern Pacific. Different north–south and east–west

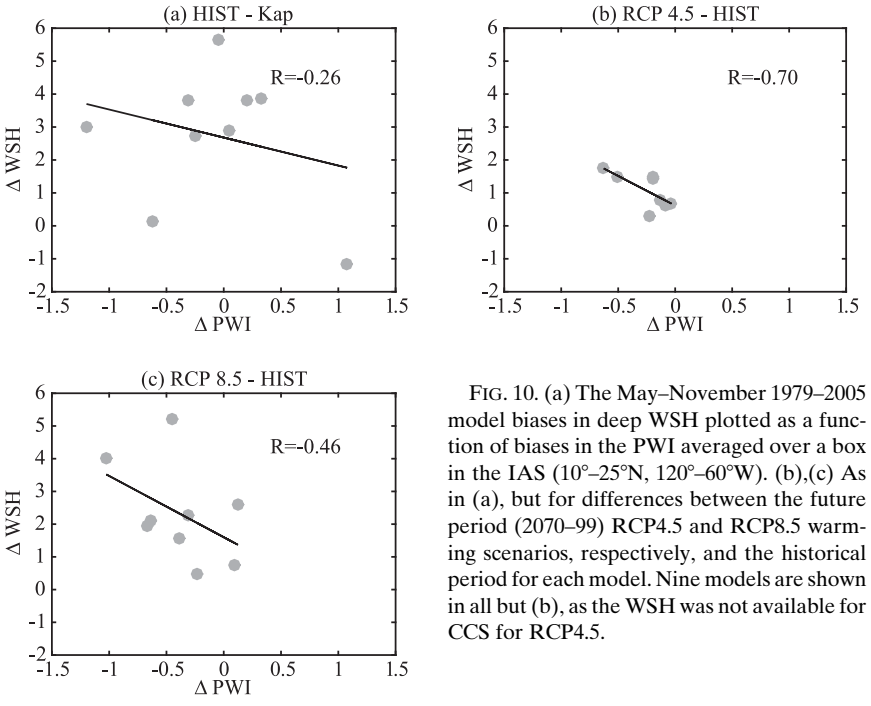

FIG. 10. (a) The May–November 1979–2005 model biases in deep WSH plotted as a function of biases in the PWI averaged over a box in the IAS (10°–25°N, 120°–60°W). (b),(c) As in (a), but for differences between the future period (2070–99) RCP4.5 and RCP8.5 warming scenarios, respectively, and the historical period for each model. Nine models are shown in all but (b), as the WSH was not available for CCS for RCP4.5.

boundaries within 5°–10° in latitude/longitude have been tested with similar results.

Examining the first column of Table 2 corresponding to the reanalysis and observations, TDEN and MSTR are both significantly correlated with SST over the region (0.32 and 0.42, respectively). The ERAI WSH is below $20\,m\,s^{-1}$ throughout the region and below $10\,m\,s^{-1}$ in the eastern Pacific (Fig. 9), suggesting mostly favorable conditions across the region for deep convection. Thus, the insignificant spatial cross correlation between TDEN and WSH in the reanalyses (−0.03) suggests that within the region WSH is sufficiently low to have no particular influence on the track distribution or strength there. Similarly, while midlevel moisture is high within the ITCZ where the TD wave tracks are most dense (Fig. 11), the spatial distribution within the region does not strongly influence wave density resulting in low but significant spatial cross correlations of TDEN with q700 (0.18). Because MSTR is shifted north of the main TD tracks (Fig. 3) where WSH tends to increase (Fig. 9) and midlevel moisture decreases (Fig. 11), spatial cross correlations of MSTR with these parameters within the region are relatively high and of the opposite sign from what is expected (0.55 and −0.43 for WSH and q700 correlations, respectively). GPI is perhaps a better measure of the overall favorable conditions for synoptic wave activity in this box, showing positive correlations with both TDEN (0.64) and MSTR (0.36) across the region, with higher correlations for TDEN than MSTR (see also Fig. 12).

The MME shows similar and significant correlations between the track parameters and SST (0.42 and 0.31 for TDEN and MSTR, respectively), indicating the strong influence of the SST on TD-wave activity in the models. As for ERAI, MME WSH throughout the region used for the calculation of the cross correlations is below $20\,m\,s^{-1}$; however, unlike for ERAI, the area of low ($\leq 10\,m\,s^{-1}$) wind shear in the eastern Pacific in the models is well correlated with the area of high MME TDEN (−0.39), perhaps suggesting an oversensitivity to this parameter in the models. On the other hand, MME MSTR shows no significant correlation with WSH (0.0). Spatial cross correlations of MME track parameters with q700 are also similar to those of ERAI (0.28 for TDEN and −0.21 for MSTR), as the spatial distribution of midlevel moisture in the models is in overall good agreement with ERAI, but with biases as discussed above. Also like ERAI, the MME GPI is the best correlated with TD-wave activity in the models (correlations of 0.67 and 0.73 for TDEN and MSTR, respectively) and even overestimates the covariability of MSTR with this parameter compared to ERAI despite showing similar or lower correlations with the individual parameters that contribute to GPI.

The spatial cross correlations of the biases in TDEN and MSTR with the biases in the MME environmental fields are also shown in Table 2. MME TDEN and

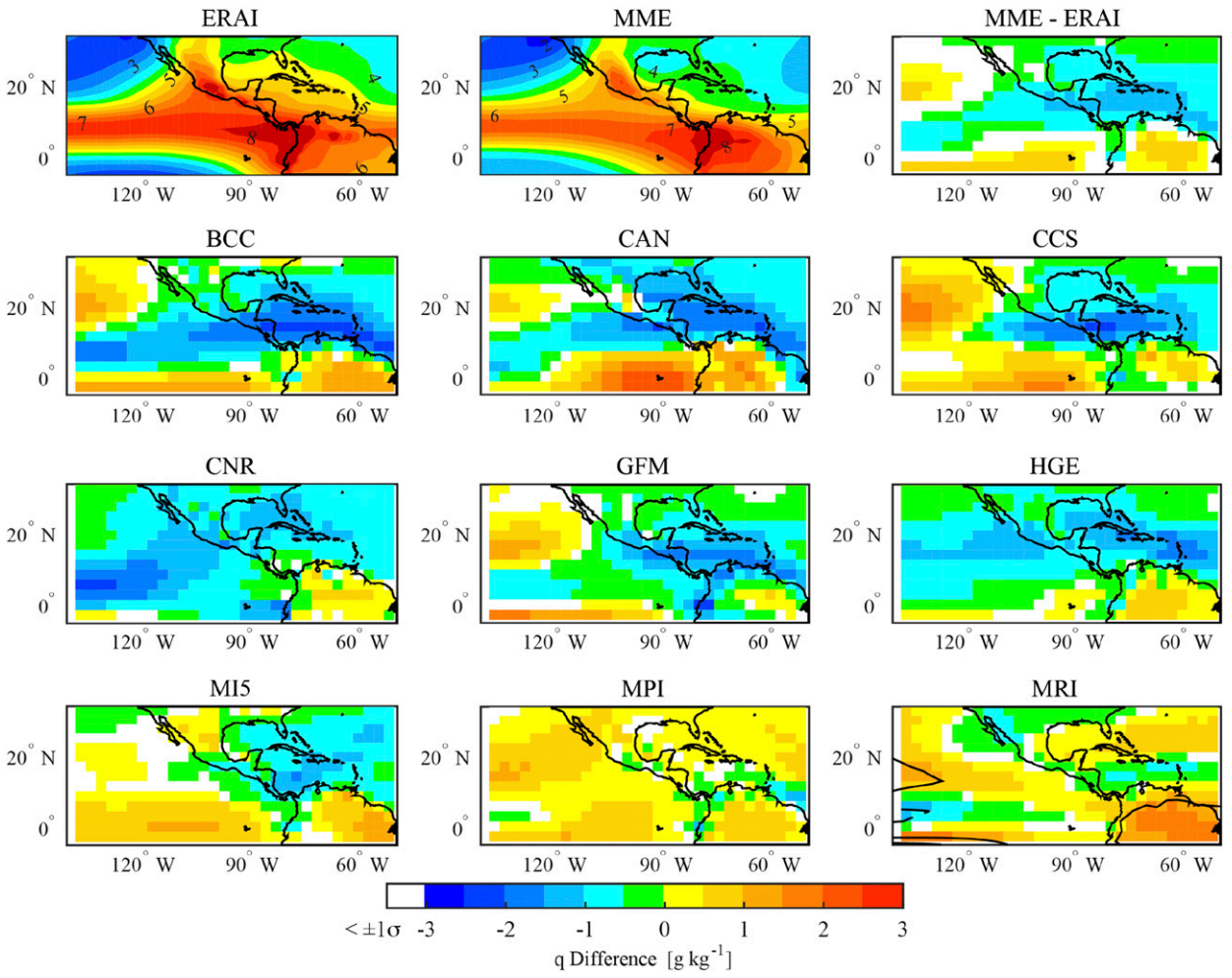

FIG. 11. As in Fig. 2, but for q700. Shaded contour interval is 0.5 g kg^{-1}.

MSTR biases are significantly correlated to biases in SST (0.46 and 0.72, respectively), with the cross correlations between the bias in MSTR and SST being notably higher than the cross correlations of the mean fields for these parameters. Cross correlations between the biases in track parameters with WSH are significant but relatively small, similar to the results for the mean fields, likely because the biases do not create mean wind shear values that significantly deter convective activity within the region. On the other hand, the cross correlations between the biases in midlevel moisture and the track parameters (0.47 for TDEN and 0.36 for MSTR) indicate that the moisture, like SST, may contribute to errors in both the TDEN and MSTR across the region. Model biases in GPI are not strongly correlated with the track parameters (0.27 for TDEN and −0.12 for MSTR) over the region despite GPI being strongly correlated with the mean TDEN and MSTR fields for the models, as discussed above. Thus, for the historical period, MME TDEN is most sensitive to biases in MME SST and midlevel moisture, while MME MSTR is most sensitive to bias in MME SST based on the environmental parameters investigated here.

c. *Future projections*

1) VORTICITY-TRACK STATISTICS

Figures 13 and 14 show the RCP8.5 MME for TDEN and MSTR for the historical and future periods, as well as the future minus historical period differences in these quantities for the MME and individual models, also presented in Sheffield et al. (2013). Overall, the models indicate a southward shift of the main wave track as well as an increase in TDEN for the future projections, consistent with results of Bengtsson et al. (2006) and Roberts et al. (2015). The region of enhanced TDEN in the future period is collocated with a

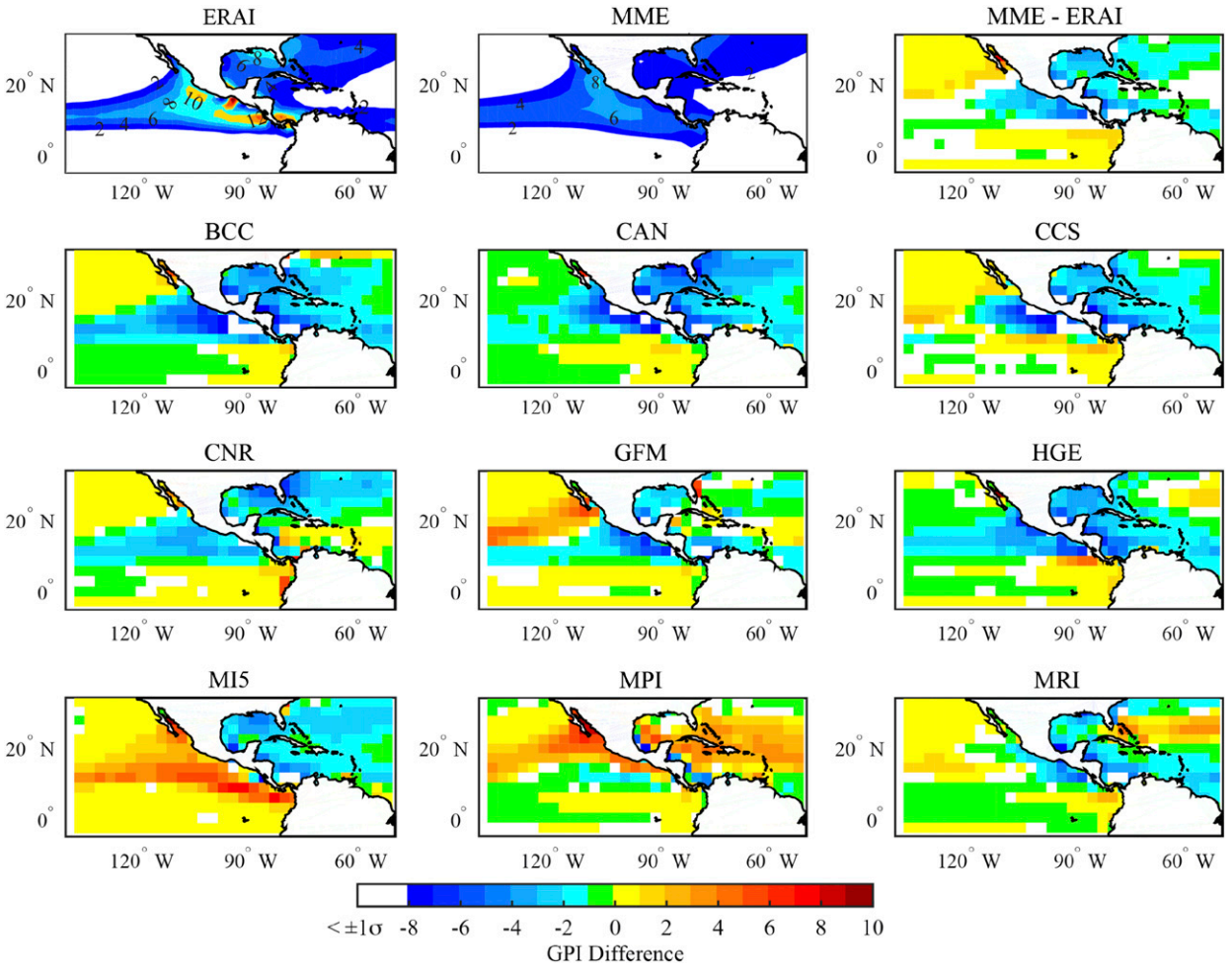

FIG. 12. As in Fig. 2, but for GPI. Shaded contour interval is 2 units for mean and 1 unit for difference.

region of positive change in MME precipitation (Fig. 15a) and GPI (Fig. 15b) and is in between regions of enhanced WSH in the eastern Pacific both near the equator and north of about 8°–10°N (Fig. 15c). The q700 changes in this region of enhanced TDEN are also positive (Fig. 15d), further supporting the shift in the wave tracks in the future. Notably, the two best-performing models for the historical period, HGE and CNR, do not show strong agreement on the magnitude of the projected future TDEN difference, but both show a southward shift.

Changes in the MSTR (Fig. 14) are overall less significant, with a region of decreased strength seen in the western Atlantic and a small region of increased strength seen in the eastern Pacific north of the main track region. Unlike for the historical period, MSTR differences show little agreement among the models for the future period, resulting in the small mean differences seen in the MME for this parameter. The difference from the historical period for each model is also generally smaller than the model historical biases shown in Fig. 3, also contributing to the lack of confidence for the MSTR changes.

Changes to the deep convective cloud activity relative to the historical period are examined using OLR (Fig. 16). CCS did not provide OLR (rlut values from the data) for the RCP8.5 future period, reducing the number of models contributing to the MME for this variable to eight in Fig. 16. The increase in deep convection south of the historical ITCZ is consistent with the overall shift in favorable environmental conditions for this activity shown in Fig. 15. A similar southward shift is also seen in TD OLR for the future period, with the maximum TD-OLR variance continuing to coincide spatially with the maximum TDEN (Fig. 17). However, while the MME TDEN shows some enhancement in the future period, the MME TD-OLR variance appears overall reduced in magnitude

TABLE 2. Spatial correlations (0°–25°N, 125°–50°W) with >95% significant correlations shown in boldface. For the historical column the Δ values indicate the bias in the MME mean with respect to ERAI WSH, ERAI GPI, or HadISST, while for the RCP8.5 column the Δ values indicate the difference between 2070–99 and 1979–2005 MME means.

	ERAI/HadISST	Historical	RCP8.5
TDEN, SST	**0.32**	**0.42**	**0.31**
MSTR, SST	**0.42**	**0.31**	**0.23**
TDEN, WSH	−0.03	**−0.39**	**−0.39**
MSTR, WSH	**0.55**	0.00	**0.20**
TDEN, q700	**0.18**	**0.28**	**0.41**
MSTR, q700	**−0.43**	**−0.21**	**0.61**
TDEN, GPI	**0.64**	**0.67**	**0.63**
MSTR, GPI	**0.36**	**0.73**	**0.68**
ΔTDEN, ΔSST	—	**0.46**	**−0.13**
ΔMSTR, ΔSST	—	**0.72**	**0.32**
ΔTDEN, ΔWSH	—	**−0.21**	**−0.46**
ΔMSTR, ΔWSH	—	**0.14**	**−0.38**
ΔTDEN, Δq700	—	**0.47**	**0.41**
ΔMSTR, Δq700	—	**0.36**	**0.61**
ΔTDEN, ΔGPI	—	**0.27**	**0.58**
ΔMSTR, ΔGPI	—	**−0.12**	**0.33**

compared to the historical period. As the total OLR fields suggest similar if not deeper convection over the ITCZ in the future (Fig. 16), the reduction in TD-OLR variance may indicate that the nature of this convection has shifted to a different region of the wavenumber–frequency spectrum in the models or that the wave energetics have changed.

2) QUANTIFYING THE RELATIVE IMPORTANCE OF ENVIRONMENTAL FACTORS IN FUTURE TD-WAVE ACTIVITY

Referring back to Table 2, the spatial cross correlations of the MME TDEN and MSTR with MME SST remain significant but somewhat reduced from the historical period (0.42 vs 0.31 and 0.31 vs 0.23, respectively), while mean SST has increased everywhere in the region (not shown). This perhaps suggests that because SST is relatively high everywhere compared to the historical simulations it supports convection associated with the waves anywhere in the region. Similarly, the horizontal structure of the positive change in SST across the region (not shown) is also not strongly correlated with TDEN changes and, in fact, shows a weak negative correlation (−0.13), suggesting that the future increases in SST in this region are in areas where the waves are suppressed because of factors other than SST. On the other hand, a significant positive correlation (0.32) is seen with the change in SST and changes in MSTR suggesting the strongest waves (potentially including TCs) remain strongly tied to areas of high SST (Table 2).

The correlations between TDEN and WSH remain unchanged (−0.39), suggesting a continued important role for low WSH in determining the location of the wave tracks, while WSH shows a slight increase in correlation with MSTR in the future (0.20). Stronger waves likely occur when WSH is low, but these systems tend to head north of the main wave track where shear increases in the models on average even more than in the historical period (Fig. 15c), resulting in a low positive correlation with this parameter in the future. There is a higher correlation of q700 with TDEN (0.41) and MSTR (0.61) in the future, suggesting that the horizontal distribution of midlevel moisture across the region remains important to the location and strength of wave activity in the models. Figure 15 suggests that the changes in WSH and, to some extent, q700 are important for establishing the shift in the wave tracks, which is further supported by the strong correlations between the changes in these fields and changes in TDEN listed in Table 2.

As WSH appears to play an important role in establishing the horizontal distribution of TD waves in both the historical and future periods for these models, we examine the correspondence between the projected changes in WSH and PWI, as in Vecchi and Soden (2007) for CMIP3. Figures 10b and 10c show the dependence of WSH changes over the region on model changes in PWI between the future and historical periods for the RCP4.5 and RCP8.5 warming scenarios, respectively. These results suggest that changes in PWI in the future period are highly correlated with changes in WSH for the group of models examined here for both the RCP4.5 (−0.70) and RCP8.5 (−0.46) warming scenarios. Thus, while the historical period biases in WSH show a weak but negative correlation to biases in model PWI, projected changes in WSH are strongly and negatively correlated with changes in the Pacific Walker cell, as found by Vecchi and Soden (2007, their Fig. 2) for CMIP3 over the western Atlantic (−0.71).

The spatial cross correlation of the track parameters with GPI remains similar in the future period, as indicated by the relatively high correlation of these fields in Table 2. Figure 15 and Table 2 further suggest that the southward shift in the maximum GPI is spatially well correlated with the southward shift in the TDEN maximum for the future period. It is important to point out that while the relationship of TDEN to GPI remains similar in the future period, the relationship of TC genesis frequency to GPI may not. In fact, as noted by the review article of Camargo and Wing (2016), the relationship between changes in model TC genesis frequency in the future and changes in GPI is not consistent, motivating the development

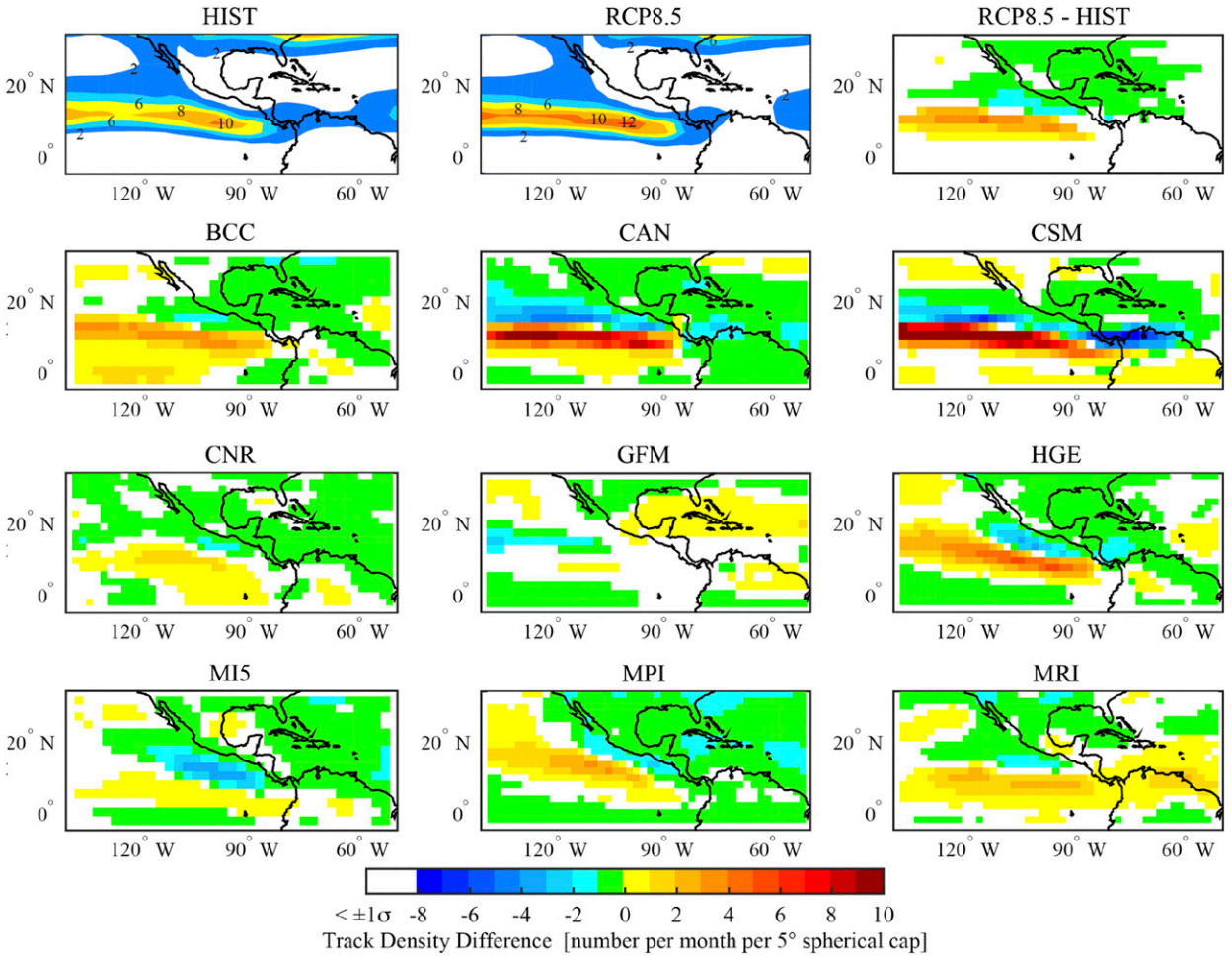

FIG. 13. The multimodel ensemble track density at 850 hPa for the (top left) historical and (top center) RCP8.5 future scenarios and (top right) their difference. The remaining panels are differences in individual models with respect to the historical period. Only differences that exceed one standard deviation of the mean based on the historical period are shaded. Track density difference shaded contours are every 1 count per month per 5° spherical cap.

of new TC genesis indices (Camargo et al. 2007; Emanuel 2010; Tippett et al. 2011; Chauvin and Royer 2010). As our ability to assess TC genesis in models improves, we will be better situated to assess the relationship between the synoptic waves and TCs in a changing climate.

In summary, while the historical period biases in TDEN are primarily associated with SST and midlevel moisture, the southward shift in the TDEN in the future for both RCP4.5 (not shown) and RCP8.5 is primarily associated with changes in the horizontal distribution of WSH, midlevel moisture, and GPI.

5. Conclusions

We have evaluated the ability of CMIP5 models to simulate synoptic wave activity across the IAS and eastern Pacific, whose biases were originally documented by the present authors in Sheffield et al. (2013). Overall, we find that the MME representation of both 850-hPa vorticity TDEN and MSTR is reasonable for the models examined in this study; however, there is a large spread in individual model ability. In particular, the MME is able to capture the spatial distribution of synoptic wave tracks and their overall number density reasonably well, although there are large differences among the individual models for this parameter suggesting the models continue to have difficulty representing the observed spectrum of convective activity in the tropics (Lin et al. 2008; Jiang et al. 2013; Martin and Thorncroft 2015). Thus, confidence in the MME TDEN is not high despite reasonable spatial correlations with the observations. Models have more consistent difficulty simulating the MSTR of the synoptic wave activity, with

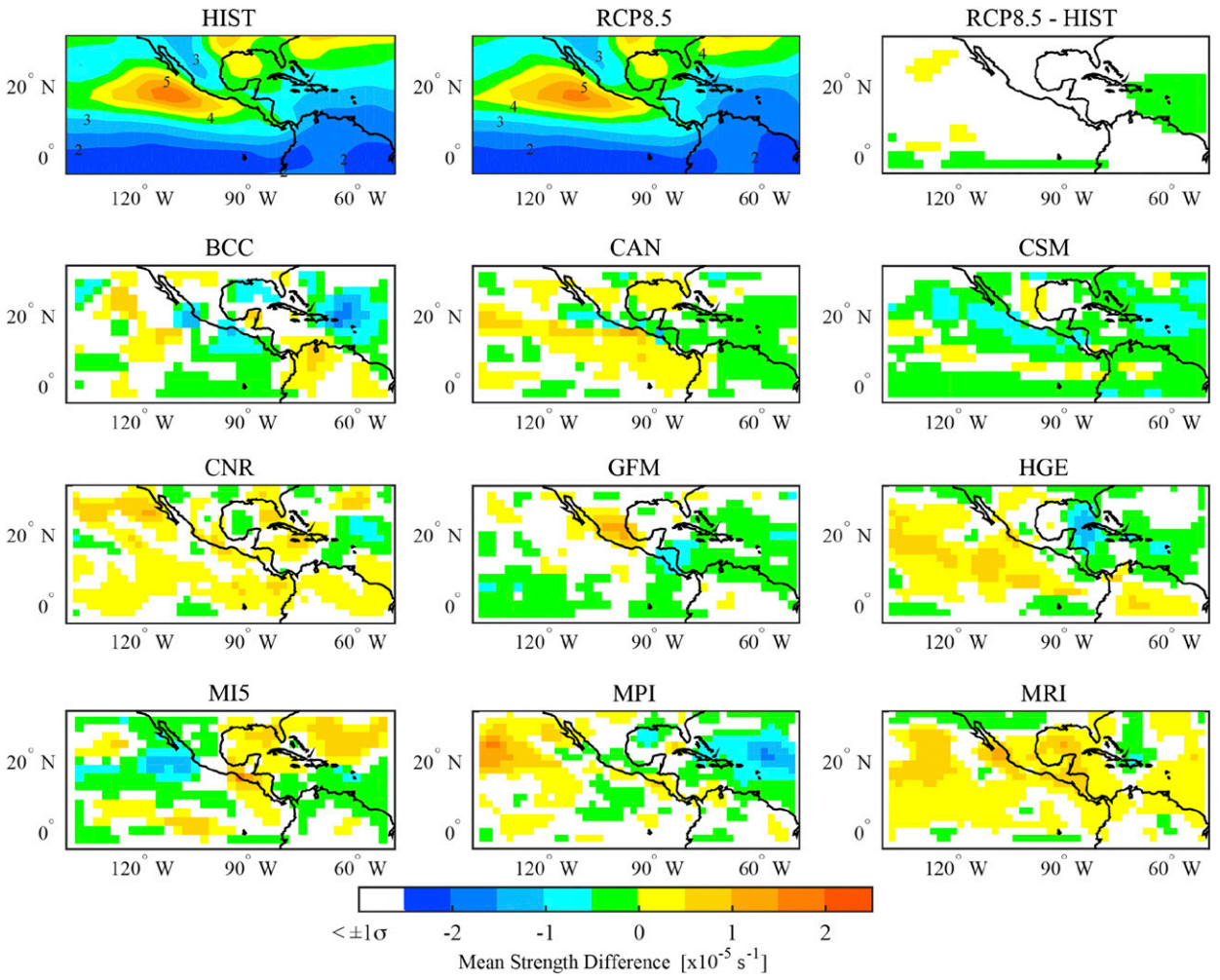

FIG. 14. As in Fig. 13, but for mean track strength. Track strength and difference shaded contours are every $0.5 \times 10^{-5}\,s^{-1}$.

nearly all models overestimating this parameter in the eastern Pacific and underestimating it along the east coast of the United States and over the Gulf of Mexico, resulting in even lower confidence in MME MSTR than TDEN.

We have also used TD-filtered OLR as an independent measure of synoptic wave activity in the models. The MME TD-filtered OLR variance is closely aligned with the MME TDEN across the region, suggesting the model low-level vorticity tracks are associated with similar wavenumber–frequency band convection as in the observations. The regions of high TDEN and TD-filtered OLR variance are also within the broader envelope of the tropical northeastern Pacific ITCZ identified by the mean OLR field in both the observations and models. As with TDEN, there is a large spread in TD-filtered OLR variance across the region among individual models, reducing the confidence in the ability of the models to represent this variance despite generally good agreement between the MME and the observations. Overall, we place higher confidence in the MME TDEN and TD-filtered OLR variability than in MME MSTR. As MSTR is shown to be most associated with TC tracks in observations, this result is perhaps not surprising given the large variability in the representation of TCs in CMIP5 (Camargo 2013). The Taylor diagrams for TDEN, MSTR, and TD OLR do not suggest that any one model outperforms the MME for the historical period. Based on this result, this study places the most confidence in the MME over any one model examined here.

Several large-scale fields have been examined to assess how sensitive the model synoptic wave activity is to known favorable large-scale conditions for the disturbances. Our results suggest that regions of high SST are well correlated with high TDEN and MSTR for the historical period and, together with regions of high GPI,

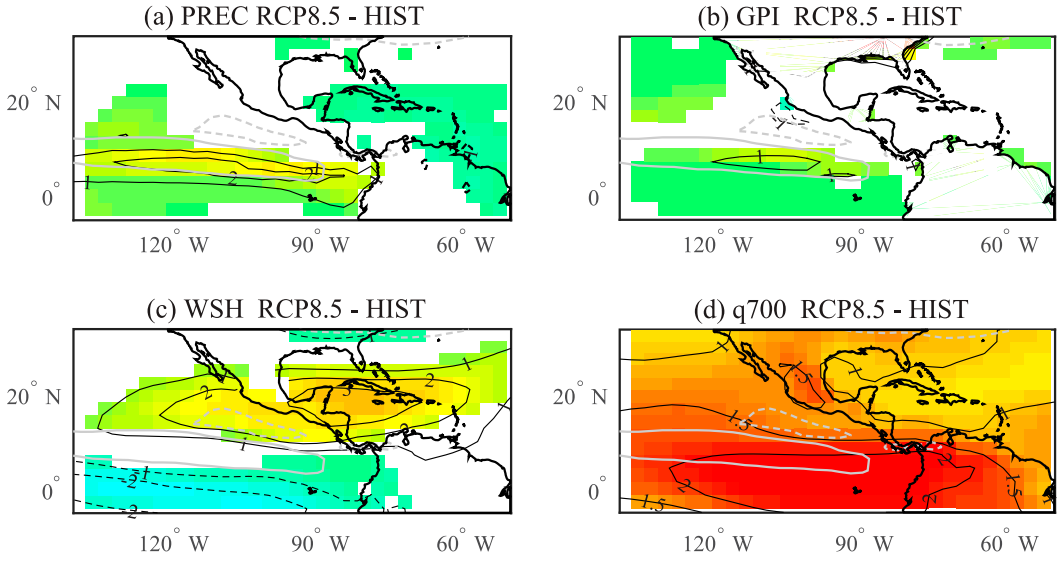

FIG. 15. The RCP8.5 multimodel ensemble mean differences with respect to the historical period for (a) precipitation (mm), (b) GPI, (c) WSH ($m\,s^{-1}$) and (d) q700 ($g\,kg^{-1}$). Contour lines indicate the magnitude of the differences, with only differences that exceed one standard deviation of the mean based on the historical period shown in color. Also shown for reference are the −1 (dashed gray) and 1 (solid gray) multimodel ensemble mean track density difference contours in units of counts per month per 5° spherical cap.

are best correlated with wave activity in both the models and reanalysis over the IAS and eastern Pacific. Model historical biases in MME track parameters are best correlated with biases in SST and midlevel moisture, suggesting there is particularly high sensitivity of the waves in the models to these parameters. This result is consistent with studies of tropical moisture modes, which predict a significant role for boundary layer moist entropy in supporting TD waves (Sobel et al. 2001; Kuang 2011; Yasunaga and Mapes 2012; Raymond et al. 2015).

Previous work has shown that the tropical eastern Pacific TD-wave tracks shift southward with global warming (Bengtsson et al. 2006). Bengtsson et al. (2006) hypothesize that, based on TDEN differences between El Niño and La Niña conditions in the current climate, the maximum warming in SST in the eastern tropical Pacific for their model likely contributes to the southward shift in the tropical wave track in this region for their study. Roberts et al. (2015) also observe a southward shift in GPI and TC tracks in their future warming experiment based on the CMIP5 HGE model, as well as a significant increase in these parameters in the central Pacific. No significant change in MSTR is found by the Bengtsson et al. (2006) study. The present study confirms the southward shift in TDEN in the far-northeastern Pacific in select CMIP5 models, with general agreement among the models providing some confidence in this result. However, changes in the MME TDEN from the historical period are not best predicted by changes in SST over the region in CMIP5 (correlation of 0.31). Instead, the analyses presented in this study suggest that areas of favorable WSH (−0.39) and midlevel moisture (0.41) best predict the geographic location of the future TDEN maximum. In addition, changes in WSH across the IAS and eastern Pacific are strongly correlated with a reduction in the PWI as found by Vecchi et al. (2006) in long climate records and by Vecchi et al. (2006) and Vecchi and Soden (2007) in CMIP3 models, linking climate changes over this region to the broader tropical Pacific basin. Similar to the Bengtsson et al. (2006) study, we find little agreement among the models for increases in MSTR for the future period. Future projections of TD-filtered OLR activity are consistent with the track statistics and suggest a southward shift of the deep convection relative to the historical simulations, providing greater confidence in this result.

The strong covariability between GPI and TDEN suggests that GPI remains a strong indicator of model synoptic wave frequency in the future climate. However, while model GPI is a reasonable predictor of observed TC genesis frequency for the present climate simulations (Camargo and Wing 2016), the relationship between model TC genesis and GPI is not consistent (e.g., Camargo 2013; Roberts et al. 2015; Camargo and Wing 2016), and thus it is difficult to draw any conclusions

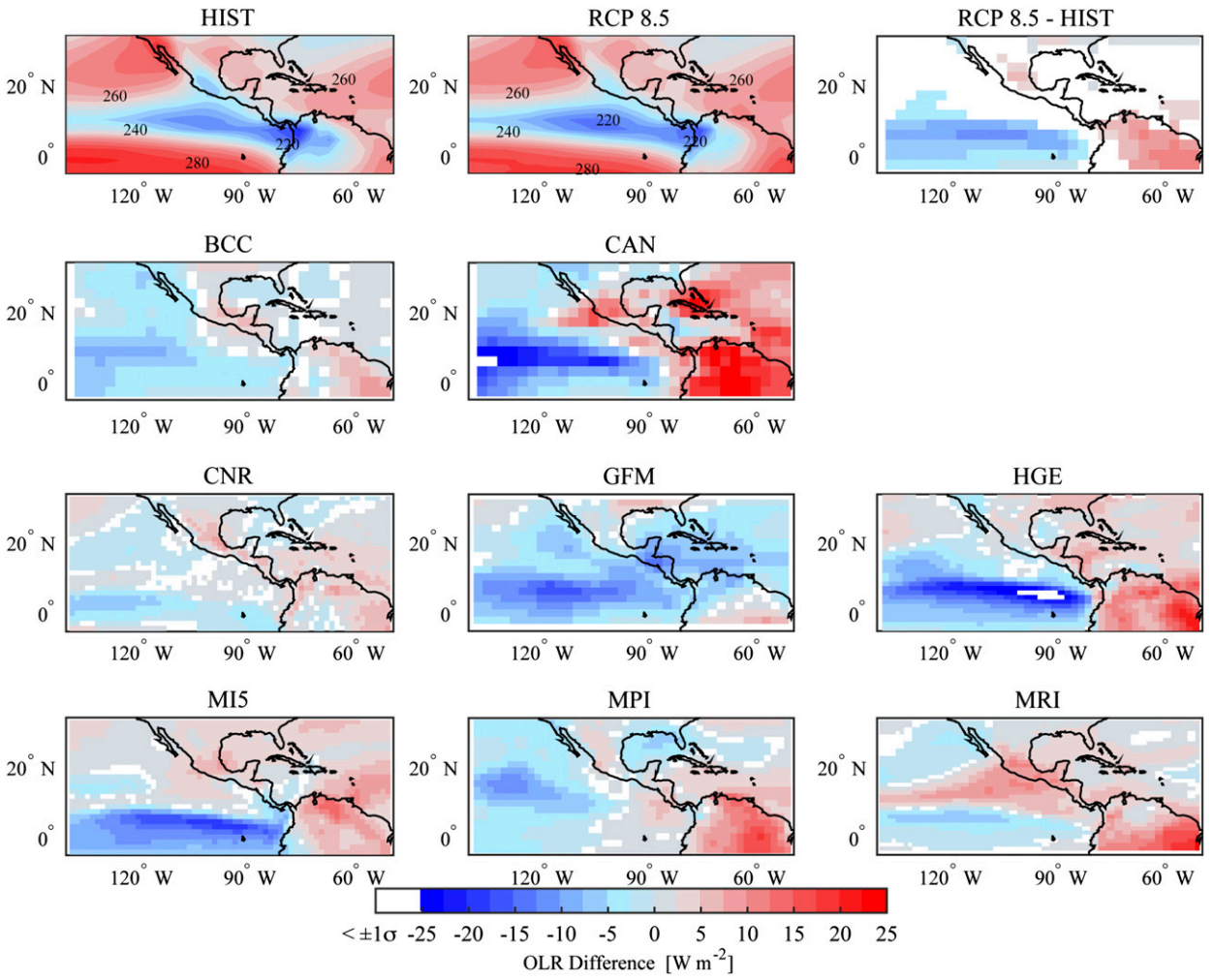

FIG. 16. As in Fig. 5, but for the future period and for eight rather than all nine models. RCP8.5 OLR fields are compared with model historical simulations. Mean (difference) field shaded contour interval is 5 (2.5) W m^{-2}.

about the shift in TD tracks and cyclogenesis in the future.

Model precipitation over the tropical northeastern Pacific also shifts southward, consistent with the shift in the TD wave tracks. This shift in TD-wave activity is not, however, associated with a significant change in precipitation over Central America for the wet season precipitation as a whole (May through November) in the models. Maloney et al. (2014) examined individual months within the wet season (June–September) and found that significant drying is observed over Central America, particularly during July and August (see their Fig. 20). Significant warming and drying over the IAS region in general is also found in earlier studies (Angeles et al. 2007; Campbell et al. 2011) and is likely in part associated with the intensification and westward extension of the NASH (Li et al. 2012). These are the months when TD-wave activity is also historically at a maximum. Overall, the intraseasonal processes controlling terrestrial precipitation over Central America are complex and involve, among other things, subgrid-scale topographic influences and convection. More study is needed, ideally using high-resolution regional modeling, to better understand the role of TD waves in establishing the intraseasonal variability of precipitation over this region and their impacts on this variability in a warmer climate. This region is of particular interest given the strong projected drying there in the future (Angeles et al. 2007; Campbell et al. 2011; Maloney et al. 2014).

Acknowledgments. The authors thank Suzana Camargo, Adam Rydbeck, and one anonymous reviewer for their helpful comments on the first draft of this manuscript. We acknowledge the World Climate Research Programme's Working Group on Coupled Modelling (WGCM), which

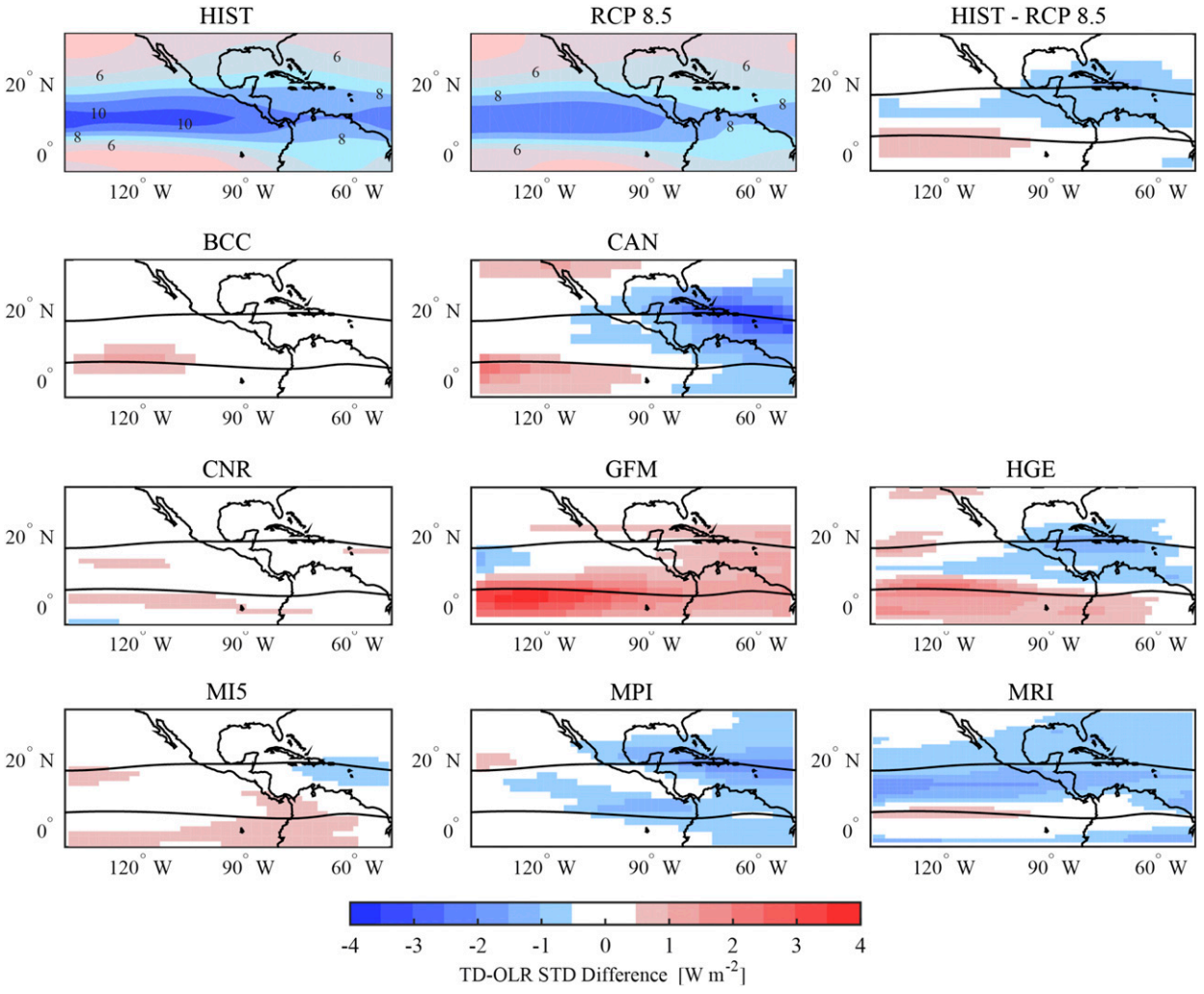

FIG. 17. As in Fig. 6, but for the RCP8.5 future period. Mean (difference) shaded contour interval is 1 (0.5) W m^{-2}. Also shown in the difference fields is the 8 W m^{-2} contour for the MME historical period for reference.

is responsible for organizing a set of coordinated climate model experiments among multiple modeling centers from around the world. The U.S. Department of Energy's Program for Climate Model Diagnosis and Intercomparison provides coordinating support and led development of software infrastructure for CMIP in partnership with the Global Organization for Earth System Science Portals. We thank the climate modeling groups listed in Table 1 of this paper for producing and making available their model output to the scientific community. This work was supported under the NOAA MAPP Program (NA10OAR4310167). Partial funding for this publication was also provided by the Joint Institute for the Study of the Atmosphere and Ocean (JISAO) under NOAA Cooperative Agreement NA10OAR4320148 (2010–2015) and NA15OAR4320063 (2015–2020), Contribution Number 2016-01-49.

REFERENCES

Adams, J. L., and D. J. Stensrud, 2007: Impact of tropical easterly waves on the North American monsoon. *J. Climate*, **20**, 1219–1238, doi:10.1175/JCLI4071.1.

Amador, J. A., E. J. Alfaro, O. G. Lizano, and V. O. Magaña, 2006: Atmospheric forcing of the eastern tropical Pacific: A review. *Prog. Oceanogr.*, **69**, 101–142, doi:10.1016/j.pocean.2006.03.007.

Angeles, M. E., J. E. Gonzalez, D. J. Erickson, and J. L. Hernández, 2007: Predictions of future climate change in the Caribbean region using global general circulation models. *Int. J. Climatol.*, **27**, 555–569, doi:10.1002/joc.1416.

Avila, L. A., and R. J. Pasch, 1995: Atlantic tropical systems of 1993. *Mon. Wea. Rev.*, **123**, 887–896, doi:10.1175/1520-0493(1995)123<0887:ATSO>2.0.CO;2.

Basnett, T. A., and D. E. Parker, 1997: Development of the global mean sea level pressure data set GMSLP2. Hadley Centre Climate Research Tech. Note 79, 62 pp.

Bengtsson, L., K. I. Hodges, and E. Roeckner, 2006: Storm tracks and climate change. *J. Climate*, **19**, 3518–3543, doi:10.1175/JCLI3815.1.

Bretherton, C. S., and L. E. Back, 2009: On the relationship between SST gradients, boundary layer winds, and convergence over the tropical oceans. *J. Climate*, **22**, 3422–3448, doi:10.1175/2008JCLI2556.1.

Camargo, S. J., 2013: Global and regional aspects of tropical cyclone activity in the CMIP5 models. *J. Climate*, **26**, 9880–9902, doi:10.1175/JCLI-D-12-00549.1.

——, and A. A. Wing, 2016: Tropical cyclones in climate models. *Wiley Interdiscip. Rev.: Climate Change*, **7**, 211–237, doi:10.1002/wcc.373.

——, A. G. Barnston, and S. E. Zebiak, 2005: A statistical assessment of tropical cyclone activity in atmospheric general circulation models. *Tellus*, **57A**, 589–604, doi:10.1111/j.1600-0870.2005.00117.x.

——, A. H. Sobel, A. G. Barnston, and K. A. Emanuel, 2007: Tropical cyclone genesis potential index in climate models. *Tellus*, **59A**, 428–443, doi:10.1111/j.1600-0870.2007.00238.x.

——, M. K. Tippett, G. A. Vecchi, M. Zhao, and A. H. Sobel, 2014: Testing the performance of tropical cyclone genesis indices in future climates using the HiRAM model. *J. Climate*, **27**, 9171–9196, doi:10.1175/JCLI-D-13-00505.1.

Campbell, J. D., M. A. Taylor, T. S. Stephenson, R. A. Watson, and F. S. Whyte, 2011: Future climate of the Caribbean from a regional climate model. *Int. J. Climatol.*, **31**, 1866–1878, doi:10.1002/joc.2200.

Caron, L.-P., and C. G. Jones, 2012: Understanding and simulating the link between African easterly waves and Atlantic tropical cyclones using a regional climate model: The role of domain size and lateral boundary conditions. *Climate Dyn.*, **39**, 113–135, doi:10.1007/s00382-011-1160-8.

——, ——, and K. Winger, 2011: Impact of resolution and downscaling technique in simulating recent Atlantic tropical cyclone activity. *Climate Dyn.*, **37**, 869–892, doi:10.1007/s00382-010-0846-7.

Chauvin, F., and J.-F. Royer, 2010: Role of the SST anomaly structures in response of cyclogenesis to global warming. *Hurricanes and Climate Change*, J. Elsner and T. Jagger, Eds., Springer, 39–56.

Crosbie, E., and Y. Serra, 2014: Intraseasonal modulation of synoptic-scale disturbances and tropical cyclone genesis in the eastern North Pacific. *J. Climate*, **27**, 5724–5745, doi:10.1175/JCLI-D-13-00399.1.

Daloz, A. S., F. Chauvin, K. Walsh, S. Lavender, D. Abbs, and F. Roux, 2012: The ability of general circulation models to simulate tropical cyclones and their precursors over the North Atlantic main development region. *Climate Dyn.*, **39**, 1559–1576, doi:10.1007/s00382-012-1290-7.

Dee, D. P., S. M. Uppala, and A. J. Simmons, 2011: The ERA-Interim reanalysis: Configuration and performance of the data assimilation system. *Quart. J. Roy. Meteor. Soc.*, **137**, 553–597, doi:10.1002/qj.828.

Dunkerton, T. J., and M. P. Baldwin, 1995: Observation of 3–6-day meridional wind oscillations over the tropical Pacific, 1973–1992: Horizontal structure and propagation. *J. Atmos. Sci.*, **52**, 1585–1601, doi:10.1175/1520-0469(1995)052<1585:OODMWO>2.0.CO;2.

——, M. T. Montgomery, and Z. Wang, 2009: Tropical cyclogenesis in a tropical wave critical layer: Easterly waves. *Atmos. Chem. Phys.*, **9**, 5587–5646, doi:10.5194/acp-9-5587-2009.

Emanuel, K., 1995: The behavior of a simple hurricane model using a convective scheme based on subcloud-layer entropy equilibrium. *J. Atmos. Sci.*, **52**, 3960–3968, doi:10.1175/1520-0469(1995)052<3960:TBOASH>2.0.CO;2.

——, 2010: Tropical cyclone activity downscaled from NOAA-CIRES reanalysis, 1908–1958. *J. Adv. Model. Earth Syst.*, **2**, 1, doi:10.3894/JAMES.2010.2.1.

——, 2013: Downscaling CMIP5 climate models shows increased tropical cyclone activity over the 21st century. *Proc. Natl. Acad. Sci. USA*, **110**, 12 219–12 224, doi:10.1073/pnas.1301293110.

——, and D. S. Nolan, 2004: Tropical cyclone activity and global climate. Preprints, *26th Conf. on Hurricanes and Tropical Meteorology*, Miami, FL, Amer. Meteor. Soc., 240–241.

Grabowski, W. W., and M. W. Moncrieff, 2004: Moisture–convection feedback in the tropics. *Quart. J. Roy. Meteor. Soc.*, **130**, 3081–3104, doi:10.1256/qj.03.135.

Gray, W. M., 1968: Global view of the origin of tropical disturbances and storms. *Mon. Wea. Rev.*, **96**, 669–700, doi:10.1175/1520-0493(1968)096<0669:GVOTOO>2.0.CO;2.

Hodges, K. I., 1995: Feature tracking on the unit sphere. *Mon. Wea. Rev.*, **123**, 3458–3465, doi:10.1175/1520-0493(1995)123<3458:FTOTUS>2.0.CO;2.

——, 1999: Adaptive constraints for feature tracking. *Mon. Wea. Rev.*, **127**, 1362–1373, doi:10.1175/1520-0493(1999)127<1362:ACFFT>2.0.CO;2.

Holton, J. R., 1971: A diagnostic model for equatorial wave disturbances: The role of vertical shear of the mean zonal wind. *J. Atmos. Sci.*, **28**, 55–64, doi:10.1175/1520-0469(1971)028<0055:ADMFEW>2.0.CO;2.

——, J. M. Wallace, and J. A. Young, 1971: On boundary layer dynamics and the ITCZ. *J. Atmos. Sci.*, **28**, 275–280, doi:10.1175/1520-0469(1971)028<0275:OBLDAT>2.0.CO;2.

Hopsch, S. B., C. D. Thorncroft, and K. R. Tyle, 2010: Analysis of African easterly wave structures and their role in influencing tropical cyclogenesis. *Mon. Wea. Rev.*, **138**, 1399–1419, doi:10.1175/2009MWR2760.1.

Hung, M.-P., J.-L. Lin, W. Wang, D. Kim, T. Shinoda, and S. J. Weaver, 2013: MJO and convectively coupled equatorial waves simulated by CMIP5 climate models. *J. Climate*, **26**, 6185–6214, doi:10.1175/JCLI-D-12-00541.1.

Jiang, X., M. Zhao, and D. E. Waliser, 2012: Modulation of tropical cyclones over the eastern Pacific by the intraseasonal variability simulated in an AGCM. *J. Climate*, **25**, 6524–6538, doi:10.1175/JCLI-D-11-00531.1.

——, E. D. Maloney, J.-L. F. Li, and D. E. Waliser, 2013: Simulations of the eastern North Pacific intraseasonal variability in CMIP5 GCMs. *J. Climate*, **26**, 3489–3510, doi:10.1175/JCLI-D-12-00526.1.

Kim, D., and Coauthors, 2014: Process-oriented MJO simulation diagnostic: Moisture sensitivity of simulated convection. *J. Climate*, **27**, 5379–5395, doi:10.1175/JCLI-D-13-00497.1.

Kozar, M. E., and V. Misra, 2013: Evaluation of twentieth-century Atlantic warm pool simulations in historical CMIP5 runs. *Climate Dyn.*, **41**, 2375–2391, doi:10.1007/s00382-012-1604-9.

Kuang, Z., 2008: A moisture-stratiform instability for convectively coupled waves. *J. Atmos. Sci.*, **65**, 834–854, doi:10.1175/2007JAS2444.1.

——, 2011: The wavelength dependence of the gross moist stability and the scale selection in the instability of column-integrated moist static energy. *J. Atmos. Sci.*, **68**, 61–74, doi:10.1175/2010JAS3591.1.

Ladwig, W. C., and D. J. Stensrud, 2009: Relationship between tropical easterly waves and precipitation during the North American monsoon. *J. Climate*, **22**, 258–271, doi:10.1175/2008JCLI2241.1.

Landsea, C. W., 1993: A climatology of intense (or major) Atlantic hurricanes. *Mon. Wea. Rev.*, **121**, 1703–1713, doi:10.1175/1520-0493(1993)121<1703:ACOIMA>2.0.CO;2.

Li, W., L. Li, M. Ting, and Y. Liu, 2012: Intensification of Northern Hemisphere subtropical highs in a warming climate. *Nat. Geosci.*, **5**, 830–834, doi:10.1038/ngeo1590.

Liebmann, B., and C. A. Smith, 1996: Description of a complete (interpolated) outgoing longwave radiation dataset. *Bull. Amer. Meteor. Soc.*, **77**, 1275–1277.

Lin, J.-L., B. E. Mapes, K. M. Weickmann, G. N. Kiladis, S. D. Schubert, M. J. Suarez, J. T. Bacmeister, and M.-I. Lee, 2008: North American monsoon and convectively coupled equatorial waves simulated by IPCC AR4 coupled GCMs. *J. Climate*, **21**, 2919–2937, doi:10.1175/2007JCLI1815.1.

Maloney, E., and D. L. Hartmann, 2001: The Madden–Julian oscillation, barotropic dynamics, and North Pacific tropical cyclone formation. Part I: Observations. *J. Atmos. Sci.*, **58**, 2545–2558, doi:10.1175/1520-0469(2001)058<2545:TMJOBD>2.0.CO;2.

——, and M. Dickinson, 2003: The intraseasonal oscillation and the energetics of summertime tropical western North Pacific synoptic-scale disturbances. *J. Atmos. Sci.*, **60**, 2153–2168, doi:10.1175/1520-0469(2003)060<2153:TIOATE>2.0.CO;2.

——, and S. Esbensen, 2003: The amplification of east Pacific Madden–Julian oscillation convection and wind anomalies during June–November. *J. Climate*, **16**, 3482–3497, doi:10.1175/1520-0442(2003)016<3482:TAOEPM>2.0.CO;2.

——, and Coauthors, 2014: North American climate in CMIP5 experiments: Part III: Assessment of twenty-first-century projections. *J. Climate*, **27**, 2230–2270, doi:10.1175/JCLI-D-13-00273.1.

Martin, E. R., and C. Thorncroft, 2015: Representation of African easterly waves in CMIP5 models. *J. Climate*, **28**, 7702–7715, doi:10.1175/JCLI-D-15-0145.1.

Menkes, C. E., M. Lengaigne, P. Marchesiello, N. C. Jourdain, E. M. Vincent, J. Lefèvre, F. Chauvin, and J.-F. Royer, 2012: Comparison of tropical cyclogenesis indices on seasonal to interannual timescales. *Climate Dyn.*, **38**, 301–321, doi:10.1007/s00382-011-1126-x.

Molinari, J., D. Knight, M. Dickinson, D. Vollaro, and S. Skubis, 1997: Potential vorticity, easterly waves, and eastern Pacific tropical cyclogenesis. *Mon. Wea. Rev.*, **125**, 2699–2708, doi:10.1175/1520-0493(1997)125<2699:PVEWAE>2.0.CO;2.

——, D. Vollaro, S. Skubis, and M. Dickinson, 2000: Origins and mechanisms of eastern Pacific tropical cyclogenesis: A case study. *Mon. Wea. Rev.*, **128**, 125–139, doi:10.1175/1520-0493(2000)128<0125:OAMOEP>2.0.CO;2.

Moss, R. H., and Coauthors, 2010: The next generation of scenarios for climate change research and assessment. *Nature*, **463**, 747–756, doi:10.1038/nature08823.

Mozer, J. B., J. A. Zehnder, and J. B. Mozer, 1996: Lee vorticity production by large-scale tropical mountain ranges. Part II: A mechanism for the production of African waves. *J. Atmos. Sci.*, **53**, 539–549, doi:10.1175/1520-0469(1996)053<0539:LVPBLS>2.0.CO;2.

Raymond, D. J., 1995: Regulation of moist convection over the west Pacific warm pool. *J. Atmos. Sci.*, **52**, 3945–3959, doi:10.1175/1520-0469(1995)052<3945:ROMCOT>2.0.CO;2.

——, and Ž. Fuchs, 2007: Convectively coupled gravity and moisture modes in a simple atmospheric model. *Tellus*, **59A**, 627–640, doi:10.1111/j.1600-0870.2007.00268.x.

——, and ——, 2009: Moisture modes and the Madden–Julian oscillation. *J. Climate*, **22**, 3031–3046, doi:10.1175/2008JCLI2739.1.

——, G. Raga, C. Bretherton, J. Molinari, C. Lopez-Carrillo, and Ž. Fuchs, 2003: Convective forcing in the intertropical convergence zone of the eastern Pacific. *J. Atmos. Sci.*, **60**, 2064–2082, doi:10.1175/1520-0469(2003)060<2064:CFITIC>2.0.CO;2.

——, Ž. Fuchs, S. Gjorgjievska, and S. Sessions, 2015: Balanced dynamics and convection in the tropical troposphere. *J. Adv. Model. Earth Syst.*, **7**, 1093–1116, doi:10.1002/2015MS000467.

Rayner, N. A., D. E. Parker, and E. B. Horton, 2003: Global analyses of sea surface temperature, sea ice, and night marine air temperature since the late nineteenth century. *J. Geophys. Res.*, **108**, 4407, doi:10.1029/2002JD002670.

Reed, R. J., and E. E. Recker, 1971: Structure and properties of synoptic-scale wave disturbances in the equatorial western Pacific. *J. Atmos. Sci.*, **28**, 1117–1133, doi:10.1175/1520-0469(1971)028<1117:SAPOSS>2.0.CO;2.

Riehl, H., 1945: *Waves in the Easterlies and the Polar Front in the Tropics*. University of Chicago Press, 79 pp.

Roberts, M. J., and Coauthors, 2015: Tropical cyclones in the UPSCALE ensemble of high-resolution global climate models. *J. Climate*, **28**, 574–596, doi:10.1175/JCLI-D-14-00131.1.

Roeckner, E., and Coauthors, 2003: The atmospheric general circulation model ECHAM 5. Part I: Model description. Max Planck Institute for Meteorology Rep. 349, 140 pp. [Available online at http://mms.dkrz.de/pdf/klimadaten/service_support/documents/mpi_report_349.pdf.]

Rydbeck, A. V., and E. D. Maloney, 2014: Energetics of east Pacific easterly waves during intraseasonal events. *J. Climate*, **27**, 7603–7621, doi:10.1175/JCLI-D-14-00211.1.

——, ——, S.-P. Xie, J. Hafner, and J. Shaman, 2013: Remote forcing versus local feedback of east Pacific intraseasonal variability during boreal summer. *J. Climate*, **26**, 3575–3596, doi:10.1175/JCLI-D-12-00499.1.

Seastrand, S., Y. L. Serra, C. Castro, and E. A. Ritchie, 2015: The dominant synoptic-scale modes of North American monsoon precipitation. *Int. J. Climatol.*, **35**, 2019–2032, doi:10.1002/joc.4104.

Serra, Y. L., G. N. Kiladis, and M. F. Cronin, 2008: Horizontal and vertical structure of easterly waves in the Pacific ITCZ. *J. Atmos. Sci.*, **65**, 1266–1284, doi:10.1175/2007JAS2341.1.

——, ——, and K. I. Hodges, 2010: Tracking and mean structure of easterly waves over the Intra-Americas Sea. *J. Climate*, **23**, 4823–4840, doi:10.1175/2010JCLI3223.1.

Sheffield, J., and Coauthors, 2013: North American climate in CMIP5 experiments. Part II: Evaluation of historical simulations of intraseasonal to decadal variability. *J. Climate*, **26**, 9247–9290, doi:10.1175/JCLI-D-12-00593.1.

Small, R. J., S.-P. Xie, E. D. Maloney, S. P. de Szoeke, and T. Miyama, 2011: Intraseasonal variability in the far-east pacific: investigation of the role of air-sea coupling in a regional coupled model. *Climate Dyn.*, **36**, 867–890, doi:10.1007/s00382-010-0786-2.

Sobel, A. H., J. Nilsson, and L. M. Polvani, 2001: The weak temperature gradient approximation and balanced tropical moisture waves. *J. Atmos. Sci.*, **58**, 3650–3665, doi:10.1175/1520-0469(2001)058<3650:TWTGAA>2.0.CO;2.

Takayabu, Y. N., and T. Nitta, 1993: 3-5 day-period disturbances coupled with convection over the tropical Pacific Ocean. *J. Meteor. Soc. Japan*, **71**, 221–246.

Taylor, K. E., 2001: Summarizing multiple aspects of model performance in a single diagram. *J. Geophys. Res.*, **106**, 7183, doi:10.1029/2000JD900719.

Ting, M., S. J. Camargo, C. Li, and Y. Kushnir, 2015: Natural and forced North Atlantic hurricane potential intensity change in CMIP5 models. *J. Climate*, **28**, 3926–3942, doi:10.1175/JCLI-D-14-00520.1.

Tippett, M. K., S. J. Camargo, and A. H. Sobel, 2011: A Poisson regression index for tropical cyclone genesis and the role of large-scale vorticity in genesis. *J. Climate*, **24**, 2335–2357, doi:10.1175/2010JCLI3811.1.

Toma, V. E., and P. J. Webster, 2010: Oscillations of the intertropical convergence zone and the genesis of easterly

waves. Part I: Diagnostics and theory. *Climate Dyn.*, **34**, 587–604, doi:10.1007/s00382-009-0584-x.

Vecchi, G. A., and B. J. Soden, 2007: Increased tropical Atlantic wind shear in model projections of global warming. *Geophys. Res. Lett.*, **34**, L08702, doi:10.1029/2006GL028905.

——, ——, A. T. Wittenberg, I. M. Held, A. Leetmaa, and M. J. Harrison, 2006: Weakening of tropical Pacific atmospheric circulation due to anthropogenic forcing. *Nature*, **441**, 73–76, doi:10.1038/nature04744.

Vitart, F., J. L. Anderson, and W. F. Stern, 1997: Simulation of interannual variability of tropical storm frequency in an ensemble of GCM integrations. *J. Climate*, **10**, 745–760, doi:10.1175/1520-0442(1997)010<0745:SOIVOT>2.0.CO;2.

Walsh, K., S. Lavender, E. Scoccimarro, and H. Murakami, 2013: Resolution dependence of tropical cyclone formation in CMIP3 and finer resolution models. *Climate Dyn.*, **40**, 585–599, doi:10.1007/s00382-012-1298-z.

Wang, C., S.-K. Lee, and D. B. Enfield, 2007: Impact of the Atlantic warm pool on the summer climate of the Western Hemisphere. *J. Climate*, **20**, 5021–5040, doi:10.1175/JCLI4304.1.

Wang, C.-C., and G. Magnusdottir, 2005: ITCZ breakdown in three-dimensional flows. *J. Atmos. Sci.*, **62**, 1497–1512, doi:10.1175/JAS3409.1.

——, and ——, 2006: The ITCZ in the central and eastern Pacific on synoptic time scales. *Mon. Wea. Rev.*, **134**, 1405–1421, doi:10.1175/MWR3130.1.

Wheeler, M., and G. Kiladis, 1999: Convectively coupled equatorial waves: Analysis of clouds and temperature in the wavenumber–frequency domain. *J. Atmos. Sci.*, **56**, 374–399, doi:10.1175/1520-0469(1999)056<0374:CCEWAO>2.0.CO;2.

Yasunaga, K., and B. Mapes, 2012: Differences between more divergent and more rotational types of convectively coupled equatorial waves. Part II: Composite analysis based on space–time filtering. *J. Atmos. Sci.*, **69**, 17–34, doi:10.1175/JAS-D-11-034.1.

Yin, L., R. Fu, E. Shevliakova, and R. E. Dickinson, 2012: How well can CMIP5 simulate precipitation and its controlling processes over tropical South America? *Climate Dyn.*, **41**, 3127–3143, doi:10.1007/s00382-012-1582-y.

Zehnder, J. A., D. M. Powell, and D. L. Ropp, 1999: The interaction of easterly waves, orography, and the intertropical convergence zone in the genesis of eastern Pacific tropical cyclones. *Mon. Wea. Rev.*, **127**, 1566–1585, doi:10.1175/1520-0493(1999)127<1566:TIOEWO>2.0.CO;2.

Zhao, H., X. Jiang, and L. Wu, 2016: Boreal summer synoptic-scale waves over the western North Pacific in multimodel simulations. *J. Climate*, **29**, 4487–4508, doi:10.1175/JCLI-D-15-0696.1.